Homing in Scale Space

M.Sc. Thesis Draft
Submitted by: David Churchill
Submitted to: Dr. A Vardy
November 18, 2008

Contents

List of Figures

1 Introduction

Visual homing is the ability of an agent to return to a goal position by comparing the currently viewed image with an image captured at the goal, known as the snapshot image. It has been shown that insects such as bees and ants have the ability to visually home and that this is a crucial component in their overall navigational strategy [5]. Visual homing has been utilized in robotics as a means of executing learned paths [6, 7] and travelling between the nodes of a topological map [8, 9]. In this paper we propose a new visual homing method which is far less constrained than existing methods in that it can infer the direction of translation without any estimation of the direction of rotation, thus it does not require the current and snapshot images to be captured from the same 3D orientation. Existing methods for visual based homing can be classified as either holistic or correspondence [3].

1.1 Holistic Methods

Holistic methods rely on comparisons between images as a whole. An example of a holistic method is the method of Zeil et al. who posit a simple distance metric between images and implement homing as gradient descent in the space of this distance metric [10]. This method, while elegant in its simplicity, relies on the existence of a monotonic relationship between image distance and spatial distance. It also requires small exploratory movements of the robot in order to determine the gradient of the image distance function. Möller and Vardy described an alternative method based on gradient descent that removes the need for exploratory movements

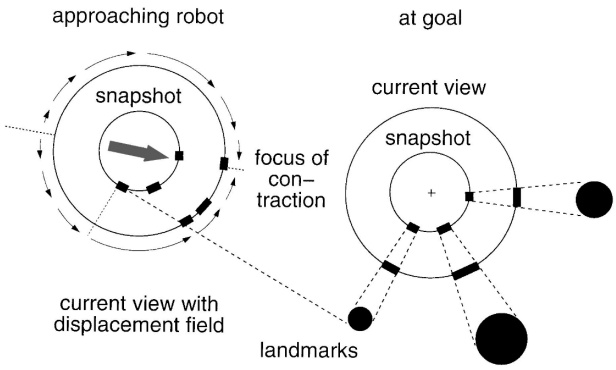

Figure 1: As the robot moves from the goal location, the surrounding landmarks seem to have displaced according to the arrows in the current view (left). If the robot moves in such a way that these displacements are minimized, it makes its way back to the goal. [1]. The warping method attempts to simulate these displacements by distorting the image based on several movement parameters [2].

prior to computing a home vector [3].

Another holistic method is the so-called *warping method* of Franz et al. [2] which searches for the parameters of motion which make the warped snapshot image most similar to the current image. A warped snapshot image is generated by transforming the snapshot image *as if* the robot had actually moved according to the given motion parameters. To make this transformation tractable the assumption is made that all objects are equidistant from the goal. Given this assumption, the resulting flow fields $\delta(\theta)$ have the following form:

$$\delta(\theta) \quad = \quad \arctan\left(\frac{\nu \sin(\theta - \alpha)}{1 - \nu \cos(\theta - \alpha)}\right) - \psi \tag{1}$$

where θ is the position of a feature in the goal image, α is the direction the robot

has moved away from the goal, ψ is the change in sensor orientation, and ν is the ratio between the average landmark distance and the true distance to the goal. The snapshot is then warped by iterating over all possible values of our movement parameters (α,ψ,ν) in order to produce an image which matches the current snapshot image. When an image is found to be a suitable match, the direction $\alpha + \pi$ is chosen as the homing direction. The algorithm for this is as follows [2]:

```
WHILE image distance to snapshot > 0 {
   FOR all values of ψ, α, ν DO {
      compute displacement field from equation (1)
      distort snapshot with displacement field
      compute image distance to current view
   }
   select parameter set with closest match
   drive in direction α + π
}
```

Despite the clearly unrealistic nature of assumption that all landmarks are of equal distance from the snapshot, the warping method has been found to perform robustly in various indoor environments. In this paper we utilize the warping method to benchmark the performance of our algorithm.

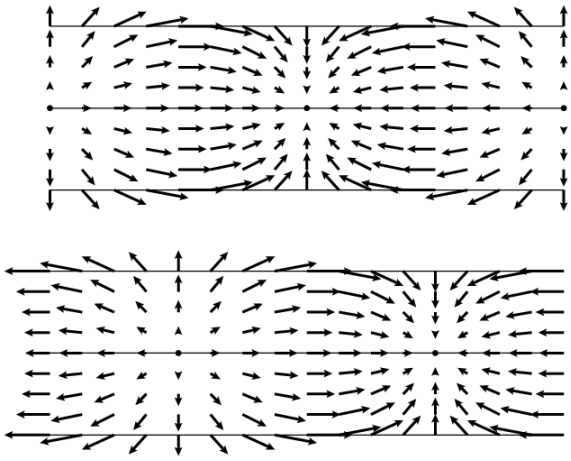

Figure 2: Ideal flow field for pure translation in a panoramic image [3].

1.2 Correspondence Methods

Correspondence based homing methods utilize feature detection and matching algorithms to form a set of correspondence vectors between the snapshot and current images. These vectors give the shift of the features in image space, known as the image flow field. The flow field formed by these correspondence vectors is then interpreted to yield the direction of motion. These flow fields comprise both robot translation as well as rotation. The separation of these two components of motion quite difficult, therefore most correspondence methods have the additional assumption that all images have identical compass orientation prior to calculating homing direction. If both the snapshot and current images are taken from the same orientation in a planar environment it is possible to compute the home direction analytically from a single correspondence vector [11]. If the orientation is not the same, one can

utilize some form of compass, or search for the change in orientation which would minimize the difference between the two images [10, 12].

One of the leading methods of visual homing is that of Vardy and Moeller [11]. Their method assumes all images have a constant orientation, and uses raw image windows as a correspondence detection method. Due to the simplicity of the windowing technique, many more matches can be attempted which compensate for lower matching accuracy. Once a set of correspondences is found, each of them is transformed into a unit homing vector via a trigonometric formula which is derived from the ideal flow field. These vectors are then summed to create a final homing vector which once normalized represents the estimated direction to the goal. While this method produces accurate results, it is constrained by the need for a stable image horizon in order for the formula to remain mathematically correct.

Various type of features have been utilized for determining correspondences, ranging in sophistication from raw image windows [11] to descriptors based on the Fourier-Mellin transform [13]. Other feature types which have been used are local features (such as corners) [14], distinctive landmarks [15], and high contrast features [1, 16, 17]. Recently, Scale Invariant Feature Transforms (SIFT) features have gained great popularity in many areas of computer vision and robotics due to the stability of their descriptor vectors with respect to changes in scaling, rotation, and illumination [4]. SIFT features have also been used to perform localization and visual homing [18, 12, 19, 20].

Pons et al [12] use SIFT landmarks in order to recover image orientation before

implementing the vector based homing strategy of Vardy and Moeller [11]. Their method uses a voting/matching scheme to minimize the horizontal component of the SIFT correspondence vectors. As we can see in Figure [x], any non-zero rotational component will extend the correspondence vectors to the left or right, raising the average horizontal length of the vectors. Two images are considered to have the same orientation when this length is minimized. This horizontal component minimization is a common technique for recovering the rotational component of image flow fields.

Biggs et al deviate from the standard two-dimensional application of SIFT feature detection by utilizing one-dimensional representations of the environment in order to reduce processing time and memory. These one-dimensional images are formed by averaging the center scanlines from the two-dimensional panoramic images. Using the snapshot and current view images as the axes of a graph, images are matched using SIFT keypoints and the resulting correspondence curve is plotted. The direction of motion required to return to the goal is then extracted from this matching curve. This method gradually builds up a world model by constant comparisons of images using this technique.

The method we will present in this thesis is similar to correspondence methods in that it relies upon finding correspondences between features. However, our interpretation of the resulting correspondences is markedly different. Consider the flow field for pure translation of an agent equipped with an omnidirectional camera. The field has a characteristic structure with foci of expansion and contraction separated by 180° (see Figure 2). If objects are distributed uniformly in the environment, half of them will appear to have expanded, while the remaining half will appear to con-

tract. Typical correspondence methods consider how the features have shifted but not whether they have expanded or contracted. The problem is that in the presence of rotation it becomes much more difficult to determine the home direction from feature shifts. Hence, the two-stage process referred to above. However, whether a feature has changed in scale is independent of any change in orientation between the two views. We utilize the change in scale of corresponding SIFT features to determine the center of the *region of contraction* which corresponds to the home direction.

We will now give a detailed explanation the SIFT feature detection process in order to full explain how our method utilizes them in order to perform visual homing.

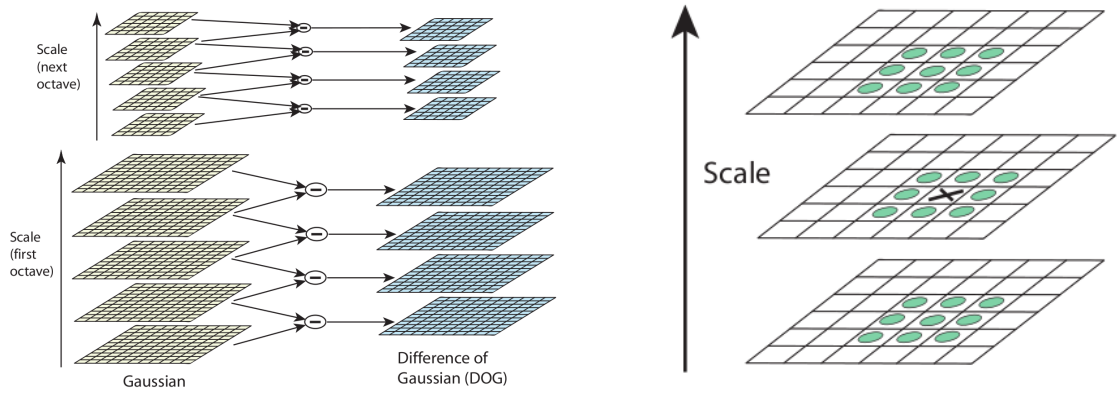

Figure 3: The original image is convolved with Gaussians to form layers of scale space (left). These layers are then subtracted to form the difference of Gaussian space. Local extrema are then detected in three dimensions within the DoG space (right) [4]

2 Scale Invariant Feature Transforms

The Scale Invariant Feature Transform (SIFT), developed by Lowe [4] is a robust image feature detection algorithm which is invariant to changes in image translation, rotation, and scale, as well as partially invariant to changes in illumination and 3D transformation. Features which the SIFT method detects are known as keypoints, and are described by a keypoint descriptor vector which contains image gradient information within a neighborhood of the keypoint. SIFT keypoints are detected and extracted via a four stage process.

The first stage of the process involves blurring the image by applying the Gaussian function G with kernel σ

$$G(x, y, \sigma) = \frac{1}{2\pi\sigma^2} e^{-(x^2+y^2)/2\sigma^2}. \quad (2)$$

The scale space $L(x, y, \sigma)$ of an image $I(x, y)$ is then the Gaussian function convolved $(*)$ with image

$$L(x, y, \sigma) = G(x, y, \sigma) * I(x, y) \tag{3}$$

Lowe's algorithm detects candidate SIFT keypoints within the Difference of Gaussian space formed by taking the difference of two of these scale space images with values of σ separated by constant multiples. That is,

$$D(x, y, \sigma) = G(x, y, k\sigma) * I(x, y) - G(x, y, \sigma) * I(x, y) \tag{4}$$

$$= L(x, y, k\sigma) - L(x, y, \sigma) \tag{5}$$

Given an initial value for σ, we apply $(G * I)$ m times with gradually increasing σ in order to obtain $m - 2$ DoG images. Image half-sizing techniques can be utilized here for optimized performance, which are discussed at length in [4]. Local minima and maxima within the DoG space are then chosen as candidate keypoints. Each point in D_n is compared to its 8 neighbors in D_n, as well as its 9 neighbors in D_{n-1} and D_{n+1}, for a total of 28 neighbor comparison.

The second stage of SIFT localizes the keypoint within the image. Accurate interpolation of sub-pixel coordinates is done by fitting a 3D quadratic function to the local sample points [4]. Also in this step, keypoints are rejected for being in areas of low contrast or poor edge response.

The third stage of SIFT assigns an orientation to each keypoint within an image.

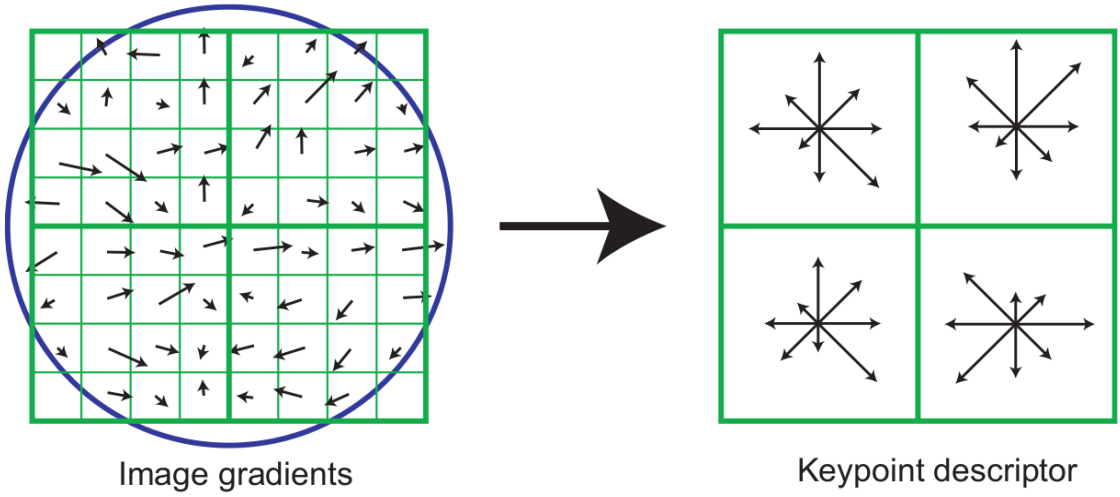

Figure 4: Local image gradients are combined into a histogram to form the SIFT keypoint descriptor vector [4]

By keeping the orientation assignment consistent with respect to the gradient within the image, keypoints can be stored with respect to their own orientation, maintaining rotation invariance among images. Since the scale σ at which the keypoint was detected is stored, we use the image $L(x, y)$ with the closest value of σ for orientation assignment, which maintains scale invariance. For each of these images, gradient magnitude and orientation are computed as

$$m(x,y) = \sqrt{(L(x+1,y) - L(x-1,y))^2 + (L(x,y+1) - L(x,y-1))^2} \quad (6)$$

$$\rho(x,y) = \tan^{-1}((L(x,y+1) - L(x,y-1))/(L(x+1,y) - L(x-1,y))) \quad (7)$$

The final stage of SIFT then computes a descriptor vector based on an orientation histogram of within a neighborhood of the keypoint. The size of this neigh-

borhood is computed with respect to σ so that scale invariance is preserved. Also, the vector is stored with respect to $\rho(x, y)$ so that the descriptor vector is invariant to rotation within the image. The descriptor vector will then be used later as the matching criterion for SIFT keypoints. Once all four stages of the SIFT algorithm have been completed, we are left with a set of keypoints of the form

$$\mathbf{f} = \{f_x, f_y, f_\sigma, f_\rho, \mathbf{f}_{kpd}\}, \tag{8}$$

where $\mathbf{f}_{kpd}$ is the keypoint descriptor vector.

2.1 Advantages

While Scale Invariant Feature Transforms have been used extensively for feature matching algorithms for many areas of robotics, for homing in scale space they are much more than just a feature matching technique. Not only do they provide an incredibly robust feature for matching, they also give us the scale σ at which they were detected. This scale space value is extremely important for homing in scale space, since it provides us with a measure of scale for the keypoint itself. By comparing the scales at which two matched keypoints were found, we can tell whether or not the feature has shrunk or grown. This method of comparing scales with then allow us to draw conclusions about the locations of the regions of expansion and contraction within the image.

The value of σ stored within a keypoint is the scale at which the keypoint became a local minima or maxima in the Difference of Gaussian space. This is effectively

the scale at which the feature had been 'blurred out of existence'. If we think of the value of σ in these terms, then for two matched keypoints **a** and **b**, we can calculate the β as:

$$\beta = a_\sigma - b_\sigma \tag{9}$$

A value of $\beta > 0$ denotes a keypoint which is smaller in b than in a. Conversely, a value of $\beta < 0$ denotes a keypoint which is smaller in a than in b. While other methods have used SIFT has a feature matching algorithm, our method is the first to use the scale space information σ for visual homing analysis.

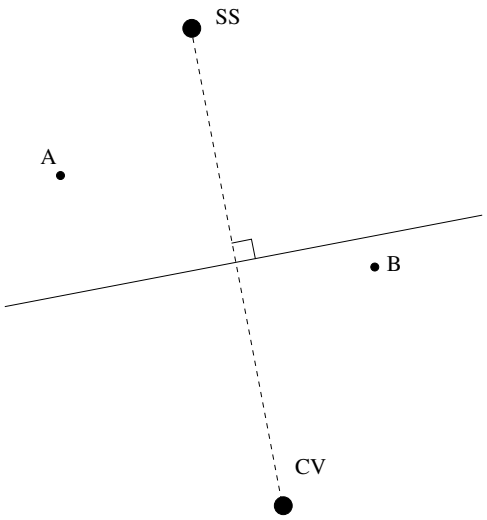

Figure 5: Robot pose diagram.

3 Homing in Scale Space

Let **CV** represent the image taken at the location (**cv**) of current panoramic view from the robot's perspective, and **SS** be the image taken at the location (**ss**) of a stored panoramic snapshot taken from the goal location.

Consider the diagram shown in Figure 5. If the robot has moved from position **ss** to position **cv**, the distance from the robot to feature A will have increased. This will be true of any feature on the same side of the perpendicular bisector of the line joining **ss** and **cv**. Similarly, the distance to the feature B will have decreased. We assume that this change in distance will be reflected in a corresponding change in the f_σ of the feature. Thus, we can classify features as either expanding or contracting. If there are sufficiently many features which are distributed evenly on either side of the dividing line then approximately half of them should experience expansion,

Figure 6: SIFT matched correspondences between **CV** (above) and **SS** (below). Correspondences in (a) show a scale decrease from **SS** to **CV**, thus having $\beta > 0$, indicating contraction. Conversely in (b) we see features which have $\beta < 0$, indicating expansion. Since these two regions should ideally be separated by π, they will be combined with a weighted average in order to more accurately compute the center of contraction.

while the other half should experience contraction. If we further assume that the features are distributed approximately uniformly throughout the environment then the home direction will be aligned with the center of the region of contraction.

Locating the center of the region of expansion / contraction from **SS** to **CV** with respect to **CV** will allow us to determine which direction the robot must head. Since **CV** is taken w.r.t. current robot orientation, not world orientation, we can then turn and move to approach the goal. We will use the change in scale information from SIFT feature correspondences to extract the center of the region of contraction, which coincides with the home direction under the assumption of uniform feature distribution.

We use panoramic images of our environment to represent views from the robot perspective. These images are w pixels wide by h pixels high. These images represent a complete viewing angle of 2π in the horizontal direction, as well as α radians in the vertical direction. Thus, each pixel represents a spacing of δ_x radians along the

x-axis, and δ_y radians along the y-axis, computable by:

$$\delta_x = \frac{2\pi}{w} \qquad\qquad \delta_y = \frac{\alpha}{h} \tag{10}$$

We therefore can convert our SIFT feature $\mathbf{f}$ with location (f_x, f_y) within the images to angular coordinates $(f_{\theta x},\ f_{\theta y})$ by

$$f_{\theta x} = f_x \delta_x \qquad f_{\theta y} = f_y \delta_y \tag{11}$$

in order to facilitate proper directional calculations.

Determining the center of the region of expansion or contraction requires detecting whether a feature has grown or shrunk with respect to its size in the snapshot image. If we revisit our SIFT feature vector, not only does it give us the location of a feature of an image, but also the scale σ at which it was detected. Therefor, given a positive SIFT match between features $\mathbf{f}_{ss}$ and $\mathbf{f}_{cv}$ with scale values of σ_{ss} and σ_{cv} respectively, we can calculate:

$$\beta \ = \ \sigma_{ss} - \sigma_{cv}. \tag{12}$$

If $\beta > 0$ then the feature has shrunk from **SS** to **CV**, and conversely if $\beta < 0$ the feature has grown. We have many keypoint correspondences, so we must compute the center of these regions of expansion and contraction in order to find the home direction.

From the correspondences in Figure 6, we can see from the matches on the right

that the desks appear to be smaller in the snapshot, while the matches on the left indicate that the filing cabinet seems to have grown. Since the cabinet represents the region of contraction in **CV**, this is the direction we wish to move. The key point of our method lies in this fact: no additional interpretation of the flow field is required. Merely the sign of β is enough to identify the change in feature size. The location of the corresponding keypoint within **SS** is not needed, since we are only concerned with the features in **CV** which have contracted. It remains for us to accurately locate the center of this region of contraction. Since the relationship between the angular orientation of **CV** and **SS** is not needed, our method achieves complete invariance to changes in relative orientation between the two images. Also, since this method does not rely on any notion of an image horizon, it is invariant to changes in relative 3D orientation and elevation. This claim will be satisfied if the following conditions hold: (1) the camera's field of view encompasses the true direction of translation, (2) a significant number of correct correspondences are found, (3) the corresponded features are approximately uniformly distributed throughout the environment.

Let us denote a matched feature pair $\mathbf{m} = (\mathbf{f}_{ss}, \mathbf{f}_{cv})$. To calculate the center of a particular region, we partition our set of correspondences $M = \{\mathbf{m}_1, \mathbf{m}_2, ..., \mathbf{m}_n\}$ into M_{pos} and M_{neg} based on the sign of β. To determine the center of these partitioned regions with respect to the robot's heading, we use the angular mean of the data,

that is: given any set of angles $\theta_1, \theta_2, ..., \theta_n$:

$$\bar{\theta}(\theta_1, \theta_2, ..., \theta_n) = \arctan\left(\frac{\sum_{i=1}^{n}\sin(\theta_i)}{\sum_{i=1}^{n}\cos(\theta_i)}\right). \quad (13)$$

We will denote the angular mean of our partitions as $\bar{\theta}_{pos}$ and $\bar{\theta}_{neg}$ respectively. We argued in section 1 that the regions of expansion and contraction are separated by π radians. We can use this fact to reduce the error in our calculation by allowing both the centers of expansion and contraction to contribute to the final result. Since both are always separated by a constant of π under ideal conditions, $\bar{\theta}_{pos} = \bar{\theta}_{neg} + \pi$.

We wish to allow both regions to contribute in such a way that a certain amount of confidence can be given to either set of data. It is often the case that $|M_{pos}|$ is significantly greater than $|M_{negs}|$, or vice versa. In an effort to assign confidence to a partition, we will use its cardinality to perform a weighted average of the mean of the data. This will shift the final calculation in the direction of the region with the most correspondences. We can compute our final home angle θ_{homing} as follows:

$$\bar{s} = |M_{pos}|\sin(\bar{\theta}_{pos}) + |M_{neg}|(\sin(\bar{\theta}_{neg}) + \pi) \quad (14)$$

$$\bar{c} = |M_{pos}|\cos(\bar{\theta}_{pos}) + |M_{neg}|(\cos(\bar{\theta}_{neg}) + \pi) \quad (15)$$

and finally:

$$\theta_{homing} = atan2\left(\bar{s}, \bar{c}\right). \quad (16)$$

This value for theta represents our final home vector with respect to the robot reference frame. Experimentally this weighted scheme has consistently shown to be more accurate than simply computing the unweighted average of the means of these regions. We summarize below our algorithm for determining the home direction:

1. Acquire an image **CV** from current robot location.
2. Perform SIFT feature matching on **SS** and **CV** to obtain a set of n matched feature pairs of the form $M = \{\mathbf{m}_1, \mathbf{m}_2, ..., \mathbf{m}_n\}$.
3. Partition M into M_{pos} and M_{neg} where pos, neg denote the sign of β from equation 3.
4. Calculate the angular means $\bar{\theta}_{pos}$ and $\bar{\theta}_{neg}$ based on the values of $f_{\theta x}$ from $\mathbf{f}_{cv}$ (i.e. the angular location of the x coordinate of the keypoint from **cv**).
5. Calculate the weighted angular mean of both $\bar{\theta}_{pos}$ and $\bar{\theta}_{neg} + \pi$ based on their cardinality as shown in equations 5-7.
6. Move the robot in the direction of the computed angle, θ_{homing}.

Sample Image	Name	Size	Grid	Spacing
	A1OriginalH	561×81	10×17	30cm
	CHall1H	561×81	10×20	50cm
	CHall2H	561×81	8×20	50cm
	Kitchen1H	583×81	12×9	10cm
	Moeller1H	583×81	22×11	10cm
	ISLab	346×50	9×8	61cm

Figure 7: Detailed information for each of the six databases used.

4 Experimental Methods

4.1 Image Databases

Several image databases were used for testing Homing in Scale Space. The images were captured in an equally spaced grid by a panoramic camera affixed to the top of a robot. In figure 9 we can see a sample of one of these panoramic images. In order to obtain the rectangular images required to perform both Homing in Scale Space, as well as the warping method, we used the unfolding algorithm available further in this section. Detailed information about each of the databases can be found in figure 7.

The A1OriginalH, CHall1H, and CHall2H databased were captured by Dr. An-

drew Vardy at the University of Bielefeld. A1OriginalH was taken at the Robot Lab Computer Eng. Group at Bielefeld, while CHall1H and CHall2H are of the main hall of the university. Kitchen1H and Moeller1H were captured by Sven Kreft and Sebastian Ruwisch, being taken in a small kitchen setting and a living room setting respectively. All of the objects in these databases remained stationary throughout the collection process. More details about these databases can be found in [21, 22].

The ISLab database was captured at the Intelligent Systems robotics laboratory at Memorial University. The setting for the database is a lab with an off white floor lit by fluorescent lighting. Since it is an active laboratory, some of the images contain people which are seen in different areas. This active setting provides for a more challenging environment for homing to take place, since some small features change locations between images. The floor of the lab is tiled by square tiles which measure 30.5×30.5cm. Images were captured at a grid equal to every second tile spacing. The area surrounding the image capture can be seen in the following floor plan:

4.2 Image Format

All images from the databases, as well as live robot trials are gray-scale panoramic images stored in portable gray map (PGM) format. Images are captured by a digital camera operating at 1024x768 pixel resolution which is pointed upward at a wide-angle hyperbolic mirror. Images taken by the camera are in a circular panoramic format as seen in figure 9. In order to perform visual homing these images must be

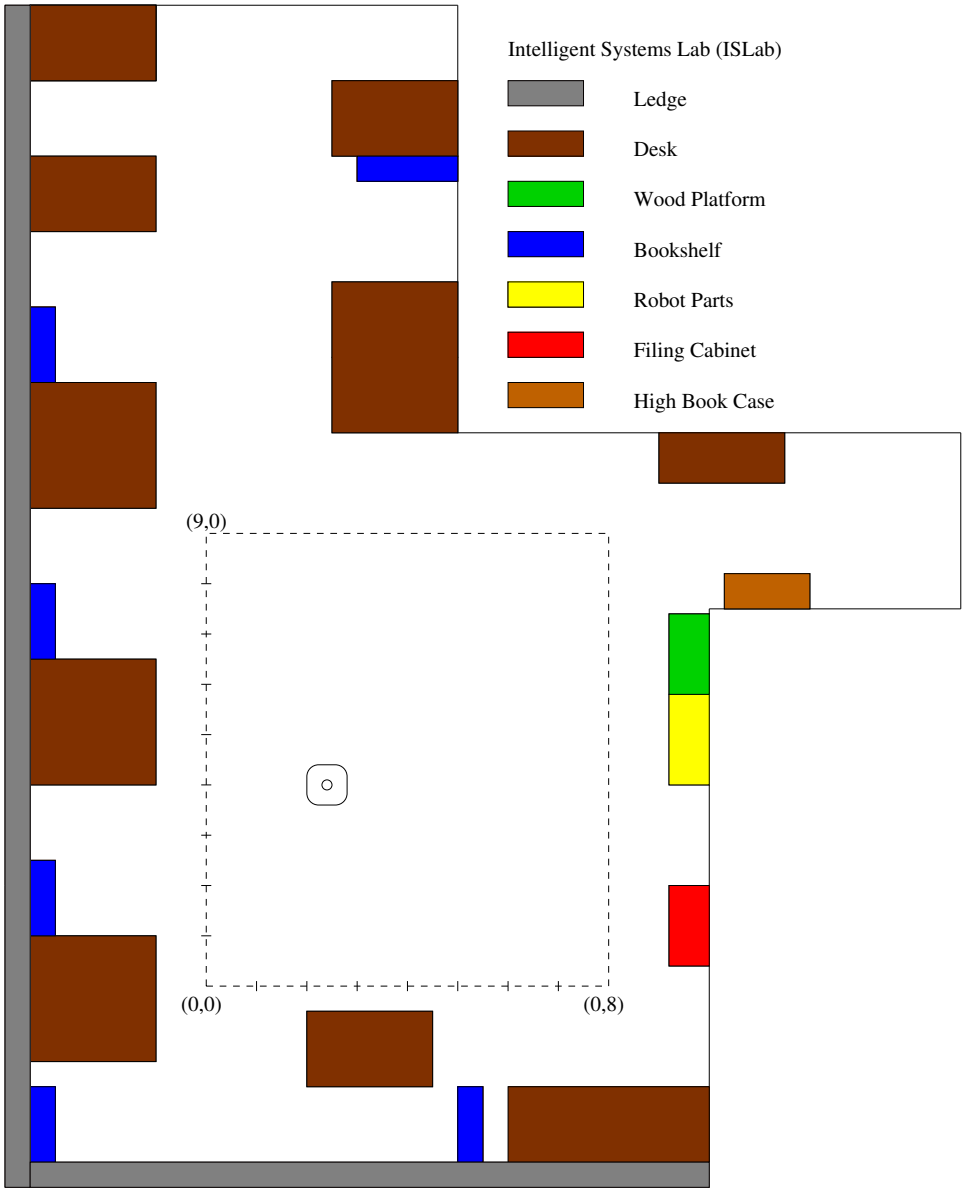

Figure 8: Diagram of the Intelligent Systems Lab at Memorial University of Newfoundland

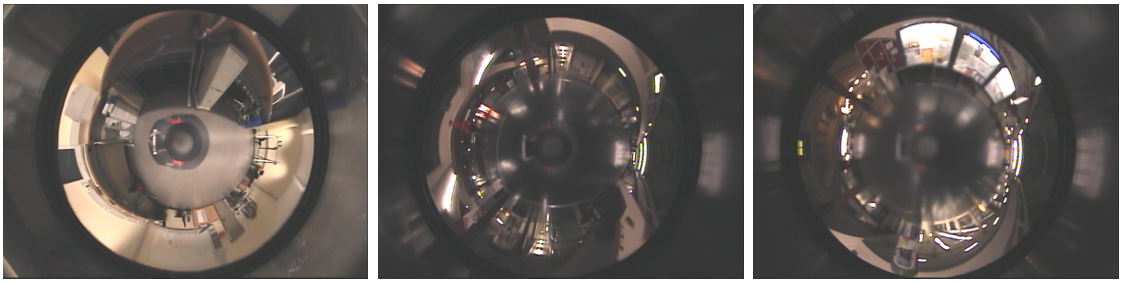

Figure 9: Panoramic images before unfolding into rectangular images. These images were taken from the A1OriginalH, CHall1H, and CHall2H databases.

transformed into rectangular coordinates by an image unfolding process as follows:

1. Determine the center point (x_c, y_c) in pixel coordinates of the input panoramic image I_p. We will treat this as the origin for I_p in terms of polar coordinates.

2. Determine the horizon of the panoramic in terms of ρ in polar coordinates.

3. Decide on a pixel resolution $w \times h$ for the output rectangular image I_r

4. Determine a sampling area ϕ about the horizon of the panoramic image to sample for the vertical portion of the rectangular image.

5. We now have our sampling frequencies in polar coordinates for the panoramic image, $\delta_\theta = \frac{w}{2\pi}$ and $\delta_\rho = \frac{h}{2\phi}$.

6. For each pixel in I_r, determine pixel (x, y) by its corresponding polar location in I_p using the sampling rate in step 5.

One known issue with this sampling process is that it produces poor resolution from point sampled near the center of the circular panoramic image. The sampling

rate δ_θ remains constant, but for smaller values of ρ near the center of the image the sampling area is much smaller, and the same pixels may be sampled multiple times. This results in a rectangular image which is much clearer near the top of the image than at the bottom.

In order to perform visual homing trials which are rotation invariant, our input images will be rotated by a random amount before each test is performed. Since each image is panoramic, they will be rotated randomly by $\theta \in [0, 360]$. To simulate this angular rotation by shifting each image with width w and height h to the right randomly by $rw \in [0, w-1]$ pixels. For some experiments we will also be simulating a random vertical shift within an image by randomly displacing it by some value $rw \in [-hr, hr]$ where $hr \in [0, h/2]$. Unlike horizontal shifting, vertical shifting will leave some portion of the image undefined, which we will fill in as black pixels. This vertical shifting will be done in order to test the robustness to shifts in the image horizon in both visual homing methods.

4.3 Programming Implementation

Implementation of the database trials for both homing in scale space as well as warping was done in C/C++. The main test framework for image reading and transformations, as well as data logging was programmed completely in C. David Lowe's SIFT implementation [4] was used for the detection and construction of SIFT keypoints for use in homing in scale space. For the warping method, we used Dr. Ralf Moeller's warping method implementation written in C++.

Figure 10: Images from the A1OriginalH database taken at location (1,1). Top image shows the original image taken by the robot. Bottom image shows the image after a random amount of rotation, plus a random vertical shift. The remaining pixels after vertical shifting are filled in with black.

Using each location in each database as a goal location, we performed both homing in scale space as well as warping methods from each other location in the database as a current location. This way we were able to exhaust each possible homing scenario from each database. Results were then stored in separate files for each database for later statistical analysis. All results graphing and statistical analysis were done using the R statistics software package [23].

Our method relies on a number of SIFT feature matches within an image in order to compute the center of a region of expansion and contraction, therefore we require as many keypoints as possible for this process. Fortunately, SIFT feature matching offers a number of parameters which can be changed in order to maximize keypoint production, while still maintaining accurate results [4]. The values changed from those of Lowe's original implementation are as follows:

1. The number of scales at which keypoints are extracted is increased from 3 to 6

to increase the number of overall keypoints, while maintaining feasible running time

2. The peak threshold for the magnitude of difference of Gaussian values is decreased from 0.08 to 0.01 in order to choose more keypoints from areas of low contrast, since indoor environments often contain such areas

3. The ratio of scores from best to second best SIFT matching has been decreased from 0.6 to 0.8. As discussed in [4], this change results in a marginal decrease in match accuracy while dramatically increasing the number of matches.

Parameters for the warping method were selected to ensure fairness with respect to running time. We selected the following values for the parameters of the warping method search space: $RhoMax = 0.95$, $RhoSteps = 36$, $AlphaSteps = 36$, and $PsiSteps = 36$ [24]. On an Intel Core2 2.13GHz processor, this parameter selection resulted in an average execution time for the warping method which was 4.8% faster per snapshot than our scale space method. We consider this to be a fair metric for results comparison.

4.4 Live Trial Implementation

Live robot trials were conducted using the Pioneer P3-AT robot [25] at the Intelligent Systems robotics lab at memorial university. The environment for the live trials was exactly the same as described for the collection of the ISLab database. To implement visual homing on the live robot we used the Advanced Robotics Interface

for Applications (ARIA) [26] robotics sensing and control libraries. ARIA is an object oriented API which provides complete control of all functions of the robot without the need for low level hardware programming. Using the MobileSim [27] software package, we were able to perform simulations of homing in scale space in a virtual environment before implementing them on a live robot. This provided for a safe, controlled way to perform debugging and analysis before performing homing in a real lab.

Utilizing ARIA on the robot allowed us to construct a simple text based interface for robot navigation and visual homing trials. Utilizing ARIA's 'safe mode' capabilities, the robot's built in ultrasonic sensors as well as laser range finders were used to stop the robot in case of imminent collisions with nearby objects in the environment. Odometry data was used during the experiments solely to turn the robot and move it forward by a certain distance after homing calculations were complete, no localization data was stored in the robot throughout the homing trials.

Five live robot trials were conducted, each of which having a fixed goal location in the environment. For each of these trials, five separate test locations were chosen in the environment to test visual homing to that particular trial's goal location. For each of these 25 tests, the following process was carried out:

1. Place the robot at the goal location for the trial.

2. Press the 'S' key to store and process the snapshot for the current goal location. For HiSS, all SIFT keypoints are computed and stored. For warping, the lookup table is constructed.

3. Navigate the robot to the desired starting location for homing

4. Press the 'C' key to start the homing process.

5. Current view image is taken, compared to the snapshot image, and the homing angle and estimated distance to goal are computed.

6. The robot turns to match the homing angle and travels the estimated distance to the goal.

7. The robot waits until a key is pressed by the user. This step was introduced in order to facilitate the recording of the position of the robot within the environment.

8. If the robot believes it is at the goal location, it ends the homing process. If it does not believe it is near the goal, it returns to step 5.

9. The test was allowed to run for a maximum of 12 iterations of steps 5-8 before manually stopping the process.

5 Results

Given two images **SS** and **CV**, the ideal visual homing algorithm computes θ_{homing}, the direction needed to move in order to reach **SS** from **CV**. The robot will then move in the direction of θ_{homing} and determine whether or not it has arrived at the goal. In order to properly measuring the accuracy of a given homing algorithm, we will require two performance metrics [11]. The first metric, known as the angular error, is the difference between θ_{homing} and the true homing direction θ_{ideal}. The second metric is the return ratio, which measures the number of times the robot was able to successfully navigate to the goal location. Both of these methods are needed due to the fact that while the correlation between angular error and return ratio is strong, a higher angular error does not *always* result in a lower return ratio. It could be the case that one method has a TAAE which is 10° higher than another, yet results in the same return ratio. It has been shown [24] that as long as the angular error remains under 90°, the robot will eventually converge to the goal location.

Each test was performed using both homing methods. Wherever 'H' or 'HiSS' is noted in a legend or table, it represents the results for the homing in scale space method. Wherever 'W' or 'Warp' is noted in a legend or table, it represents the results for the warping method. Since all tests were done with a certain level of vertical shifting, wherever 0px, 5px, 15px, or 24px is noted, it corresponds to the maximum random vertical shift for that particular trial. For example, '15H' or 'HiSS15' both refer to a trial performed by the homing in scale space method under

15 pixel maximum vertical shift.

5.1 Performance Metric

The first metric for performance evaluation we use is the average angular error between correct home vectors and our computed home vectors. Our homing method takes images located at **cv** and **ss** and returns θ_{homing}, the angle we compute to be the homing angle. Since images in the database were taken at known locations, we can compute the ideal home vector angle as follows: given the (x, y) locations of current view **cv** and a goal snapshot **ss** on an evenly spaced capture grid, we can compute

$$\theta_{ideal}(\mathbf{ss}, \mathbf{cv}) \quad = \quad atan2(\mathbf{ss}_y - \mathbf{cv}_y, \mathbf{ss}_x - \mathbf{cv}_x) \tag{17}$$

thus, the angular error AE(**ss**,**cv**) can be found by:

$$AE(\mathbf{ss}, \mathbf{cv}) \quad = \quad diff(\theta_{ideal} - \theta_{homing}) \tag{18}$$

where diff() is the true angular difference, implemented by the function

```
double diff(double a, double b)
   double diff = a - b;
   while (diff < -π) diff += 2π;
   while (diff >  π) diff -= 2π;
   return diff;
```

We can then obtain an overall average angular error as follows ($AE(\mathbf{ss}, \mathbf{ss}) = 0$):

$$AAE(\mathbf{ss}) = \frac{1}{mn}\sum_{x=1}^{m}\sum_{y=1}^{n} AE(\mathbf{ss}, \mathbf{cv}_{xy}). \quad (19)$$

Finally, to obtain a measure of performance for the entire image database we can use the total average angular error TAAE(**db**), which computes the overall average of AAE(**ss**) having computed the home direction to each possible location as the snapshot:

$$TAAE(\mathbf{db}) = \frac{1}{mn}\sum_{x=1}^{m}\sum_{y=1}^{n} AAE(\mathbf{ss}_{xy}). \quad (20)$$

The second performance metric is the return ratio. Given an environment, we say a particular attempt at homing was a success if the agent was able to return to within a given distance threshold of the goal location from its current location. Given an image database, we will determine the return success from **cv** to **ss**, $RET(\mathbf{CV}, \mathbf{SS})$ with the following method:

1. Given images **CV** and **SS** from a grid of images with locations ($\mathbf{cv}_x$,$\mathbf{cv}_y$) and ($\mathbf{ss}_x$,$\mathbf{ss}_y$) respectively, calculate θ_{homing}.

2. Calculate $\mathbf{cv}_{new} = (\mathbf{cv}_x + \cos(\theta_{homing}), \mathbf{cv}_y + \sin(\theta_{homing})$. This is the grid space pointed to by θ_{homing} from **CV**.

3. If $\mathbf{cv}_{new} = \mathbf{ss}$, homing is successful. If $\mathbf{cv}_{new}$ is outside the boundary determined by the image grid, or is the same as a previously visited **cv** (loop),

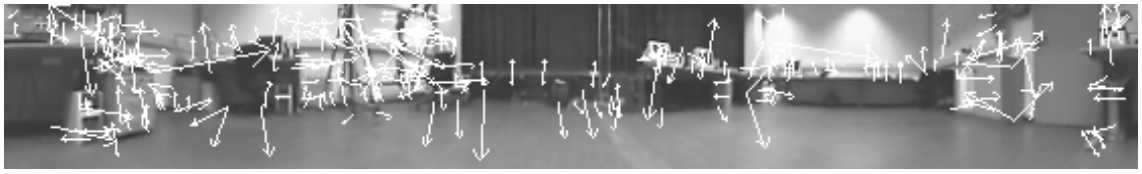

Figure 11: Sample SIFT keypoints including scale and orientation. Image taken from A1OriginalH database. Parameters were changed to detect fewer keypoints in this image for illustration purposes only.

homing is a failure. Otherwise, return to step with $\mathbf{cv} = \mathbf{cv}_{new}$.

If we iterate this process using each of the locations within the database as the goal location, attempting to return to it from each of the other locations within the database, we can determine the total return ratio $TRR(\mathbf{db})$ as the percentage of those which succeeded. If we define $RET(\mathbf{CV}, \mathbf{SS})$ as 1 for success, and 0 for failure, we can then calculate the return ratio and total return ratio as

$$RR(\mathbf{ss}) = \sum_{x=1}^{m}\sum_{y=1}^{n} RET(\mathbf{cv}_{xy}, \mathbf{ss}_{xy})/mn \quad (21)$$

$$TRR(\mathbf{db}) = \sum_{x=1}^{m}\sum_{y=1}^{n} RR(\mathbf{ss}_{xy})/mn. \quad (22)$$

5.2 Sample Results

Figures 12 and 13 are of typical correspondence vector sets generated between a current view and snapshot image. These two figures have been aligned with the same orientation for ease of interpretation. The middle image represents the current view, bottom image represents the snapshot image, while the top image shows the

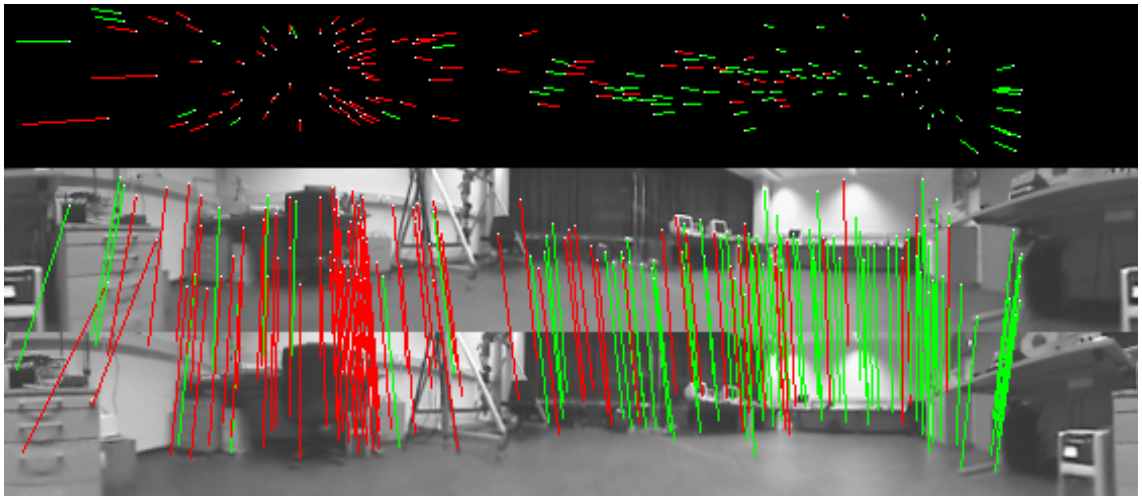

Figure 12: Sample correspondence vector image.

overlayed vector field image. Red vectors represent the contracted features while green vectors represent expanded features.

Figure 13 shows the weighted averaging scheme implemented by homing in scale space. The yellow square represents the computed center of the region of contraction $\bar{\theta}_{pos}$ while the blue square represents the center of the region of expansion $\bar{\theta}_{neg}$. The red square shows the weighted average of $\bar{\theta}_{pos}$ and $\bar{\theta}_{neg} + \pi$ which has been shifting to the right due to the higher confidence placed in the larger set of green vectors. This value is closer to the true homing direction (pink square) than the simple average.

In figure 14 we see the results of homing to location $(2, 3)$ in the A1OriginalH database from every other location in the database. Computed homing angles are represented by unit vectors in the diagram. These homing vector fields give a very good representation of the overall performance of homing to a particular location.

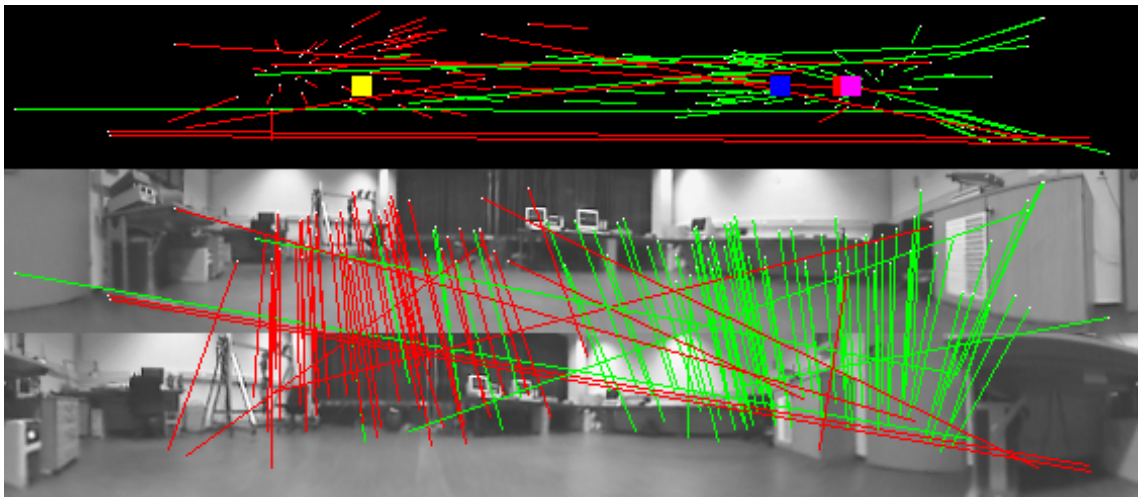

Figure 13: Illustration of the weighted mean process which takes place in homing in scale space.

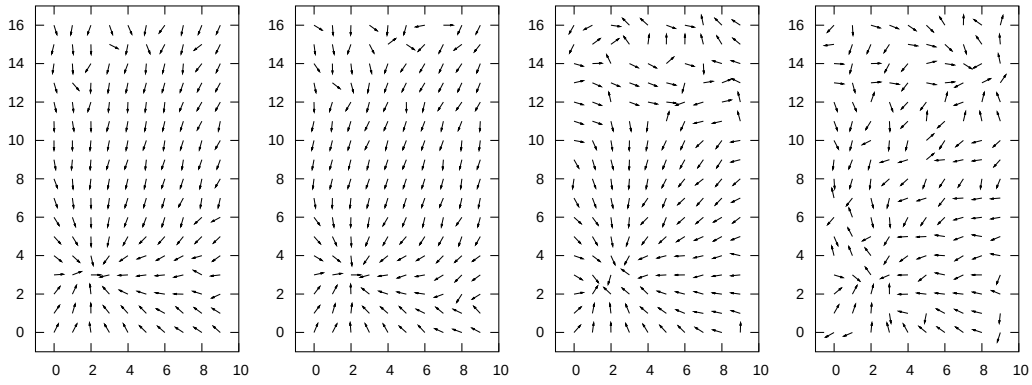

Figure 14: Homing vector images with goal position set to $(2, 3)$. First two images show scale space homing with horizontal shift only (first, AAE=12.3°) and combined vertical shift (second, AAE=18.1°). Last two images show warping method for horizontal shift only (third, AAE=39.2°) and combined vertical shift (fourth, AAE=59.4°)

Figures 15 and 16 are of grayscale grids plotted for each (x, y) location within each database. The gray scale value for a particular location within a database is scaled from black (0) to white (maximum of $TAAE(hiss), TAAE(warping)$ for the particular database). This view allows us to see which locations in a particular environment perform well (darker), or poorly (lighter). Keep in mind the aspect ratio for these figures is not 1:1, refer to the axis for coordinate information.

5.3 Angular Error - Return Ratio

In the case of the return ratio metric, our data is binary, so the higher percentage success rate is sufficient to show that our method outperformed the warping method. While the TAAE for homing in scale space is overall lower than that for the warping method, we must now show that there is indeed a significant difference between the two sets of results using statistical analysis. Certain statistical methods only work properly given an input data set which is normally distributed. In order to determine which tests to perform, we must first determine whether or not our data is normally distributed. Most statistical tests output what is known as a P-value. This P-value is the probability of obtaining a result which is at least as extreme as the one observed, given the null hypothesis is true. For the angular error data, we will use the Shapiro-Wilk, or W normality test [28, 29]. For this test, our data is considered to be not normally distributed for output values for $p < 0.1$ [30]. Upon running the W test for each of the data sets individually, as well as all combined data sets as a whole, each test returned a result of $p < 2.2e-16$, concluding that our

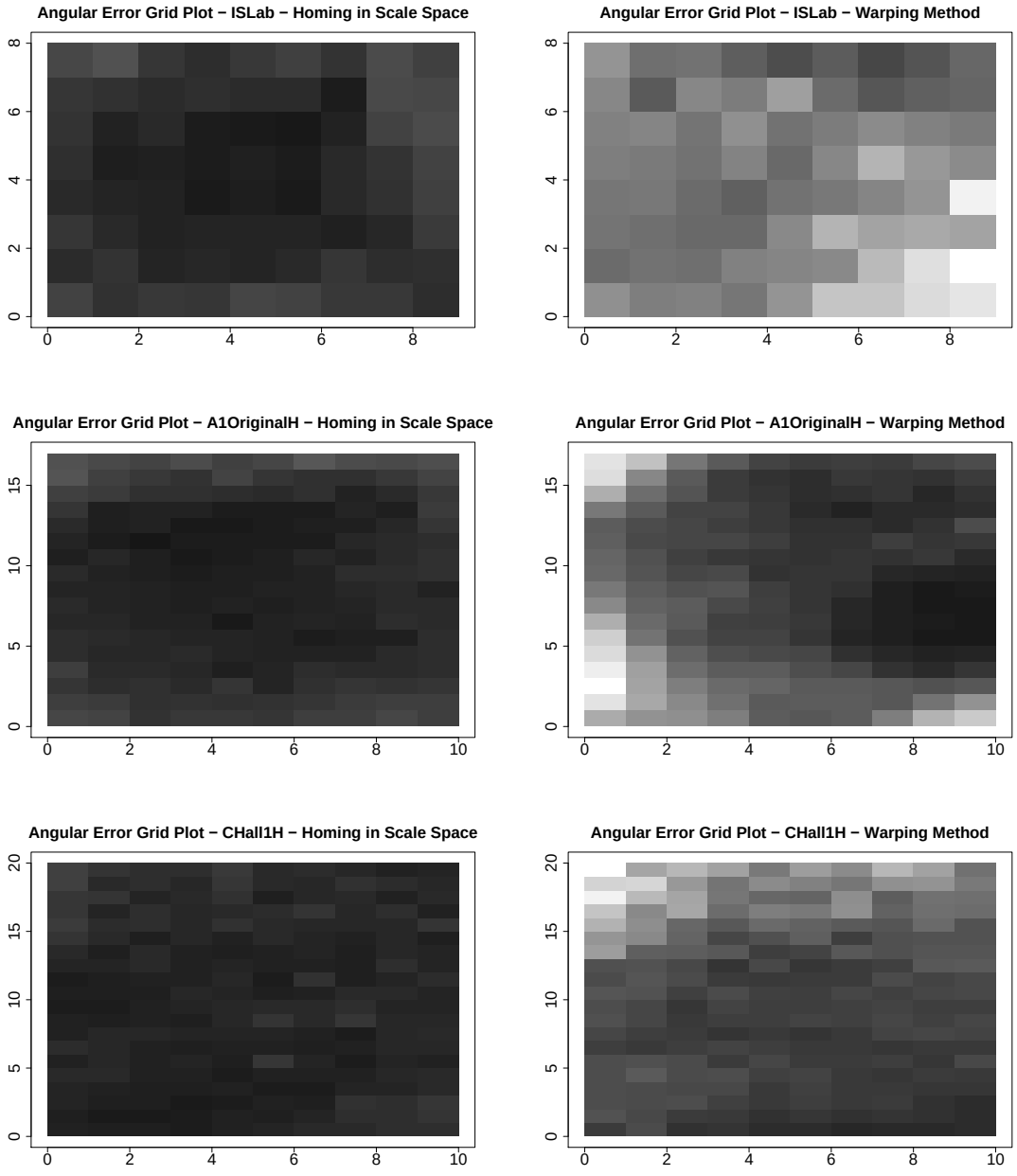

Figure 15: Grids showing TAAE results for ISLab, A1OriginalH, and CHall1H databases.

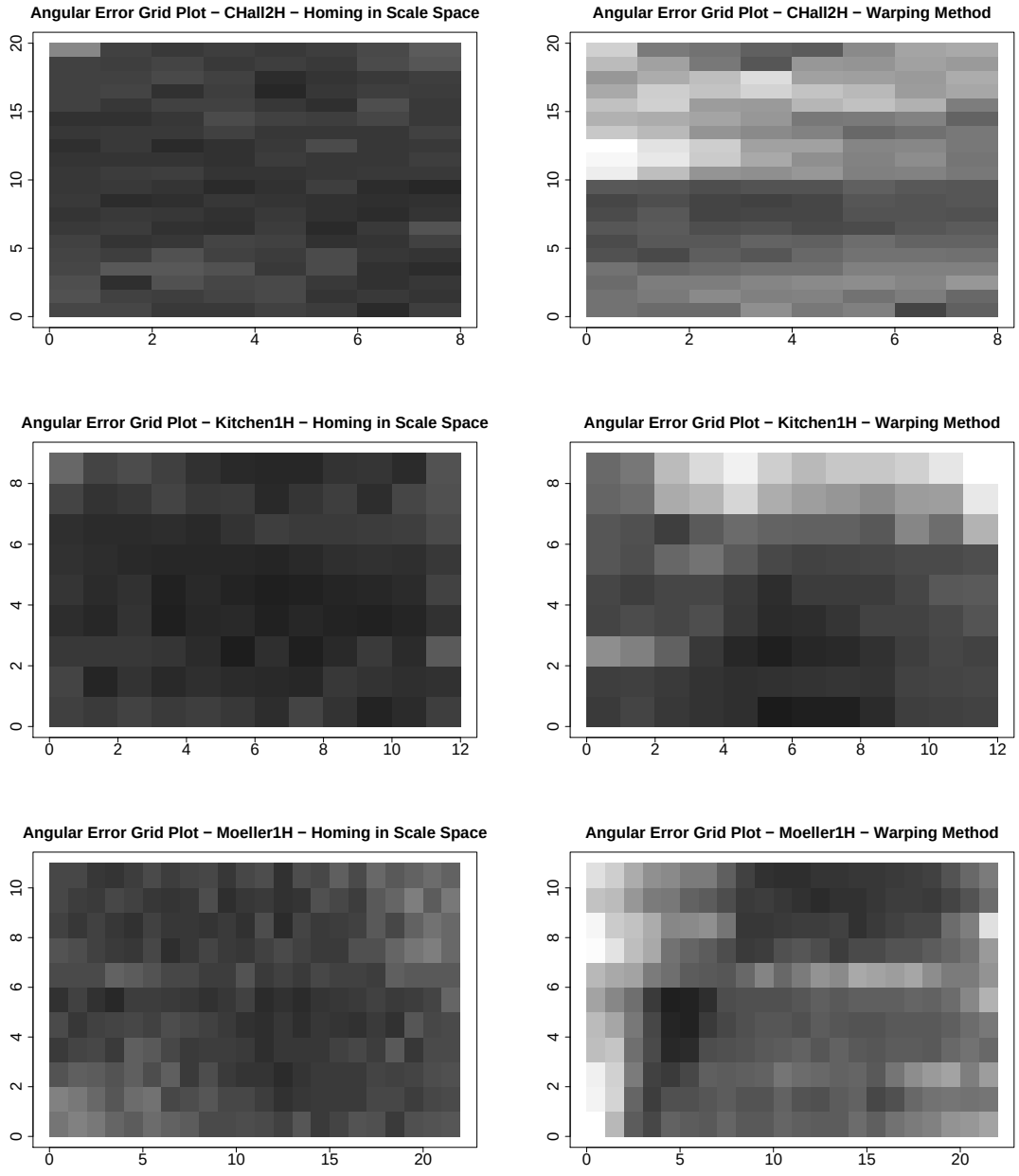

Figure 16: Grids showing TAAE results for CHall2H, Kitchen1H, and Moeller1H databases.

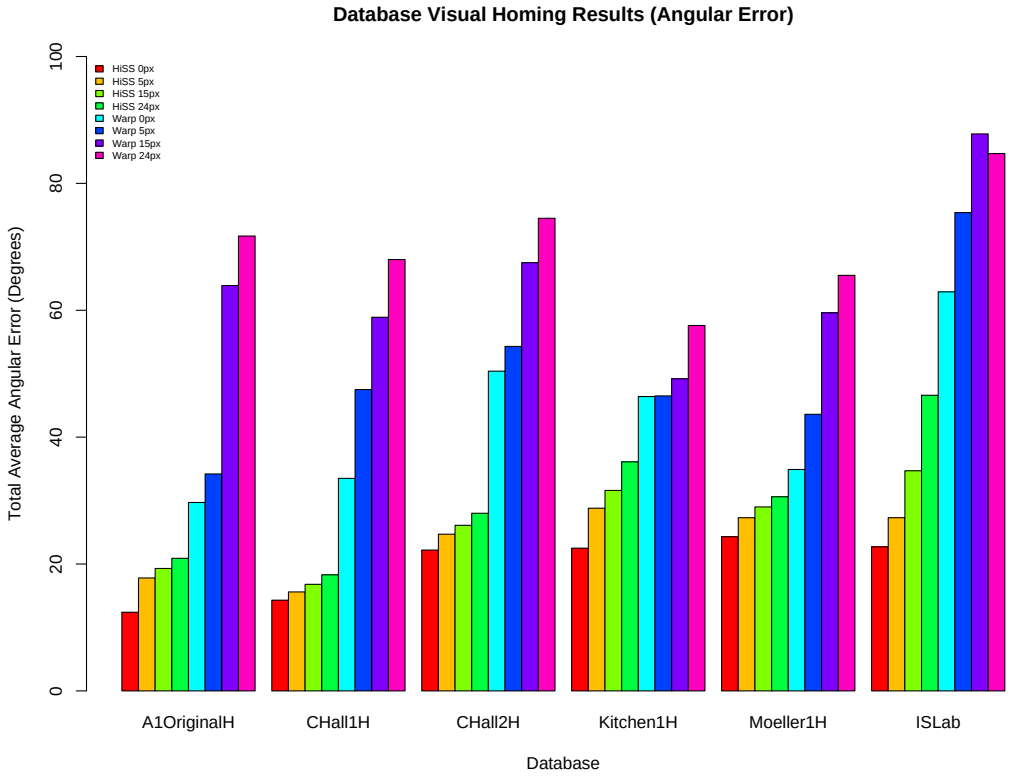

Database	0H	5H	15H	24H	0W	5W	15W	24W
A1originalH	12.4°	17.8°	19.3°	20.9°	29.7°	34.2°	63.9°	71.7°
Chall1H	14.3°	15.6°	16.8°	18.3°	33.5°	47.5°	58.9°	68.0°
Chall2H	22.2°	24.7°	26.1°	28.0°	50.4°	54.3°	67.5°	74.5°
Kitchen1H	22.5°	28.8°	31.6°	36.1°	46.4°	46.5°	49.2°	57.6°
Moeller1H	24.3°	27.3°	29.0°	30.6°	34.9°	43.6°	59.6°	65.5°
RobISLab	22.7°	27.3°	34.7°	46.6°	62.9°	75.4°	87.8°	84.7°

Figure 17: Database Results - Angular Error

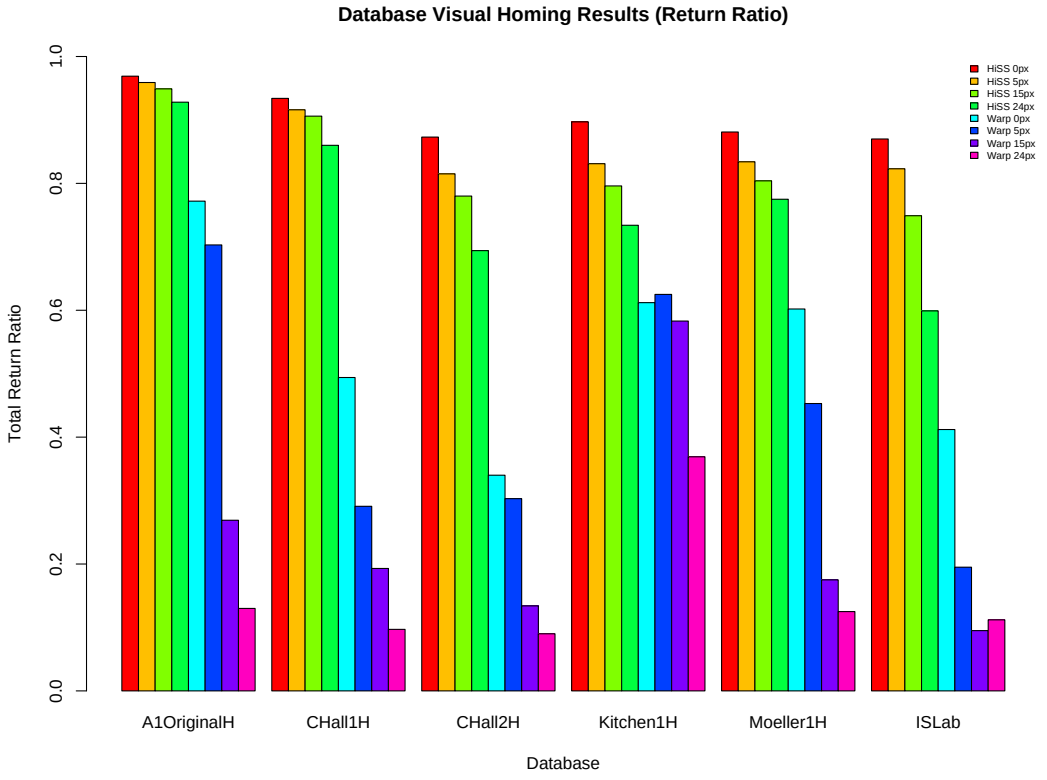

Database	0H	5H	15H	24H	0W	5W	15W	24W
A1originalH	0.969	0.959	0.949	0.928	0.772	0.703	0.269	0.130
Chall1H	0.934	0.916	0.906	0.860	0.494	0.291	0.193	0.097
Chall2H	0.873	0.815	0.780	0.694	0.340	0.303	0.134	0.090
Kitchen1H	0.897	0.831	0.796	0.734	0.612	0.625	0.583	0.369
Moeller1H	0.881	0.834	0.804	0.775	0.602	0.453	0.175	0.125
RobISLab	0.870	0.823	0.749	0.599	0.412	0.195	0.095	0.112

Figure 18: Database Results - Return Ratio

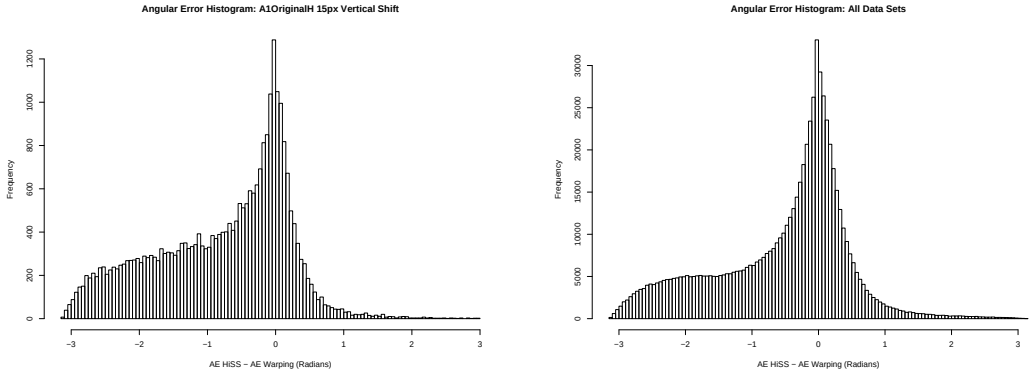

Figure 19: Angular error difference histogram. X-Axis value is angular error of homing in scale space minus that of the same trial for the warping method. The histogram shows a skew to the left side of 0, indicating an overall better performance for homing in scale space. Visual inspection along with the Shapiro-Wilk normality test concludes that the data set is not normally distributed.

data is not normally distributed. For this reason, we will use the sign test in order to draw conclusions about our angular error results. In statistics, the sign test [31] is used to determine whether or not there is 'no difference' between two variables X and Y. The output of this test is the probability that the observed values are possible given that the null hypothesis is assumed to be true. We use the sign test with the alternate hypothesis that $AE(hiss) - AE(warp) < 0$, which represents a HiSS trial which is more accurate than warping. A P-value < 0.05 is sufficient to support this alternative hypothesis [31, 32, 33].

Sign Test (With Alt. Hyp. HiSS-Warping < 0) - No Pixel Vertical Shift

Database	Samples	Mean	Median	95% CI	S-Value	P-Value
A1originalH	28900	-0.236	-0.054	$(-\pi, -0.051)$	11873	2.2e-16
Chall1H	40000	-0.318	-0.120	$(-\pi, -0.116)$	14252	2.2e-16
Chall2H	25600	-0.471	-0.255	$(-\pi, -0.246)$	8571	2.2e-16
Kitchen1H	11664	-0.375	-0.111	$(-\pi, -0.102)$	4497	2.2e-16
Moeller1H	58564	-0.197	-0.003	$(-\pi, 0.0)$	28851	0.0057
RobISLab	5184	-0.707	-0.429	$(-\pi, -0.399)$	1287	2.2e-16

Sign Test (With Alt. Hyp. HiSS-Warping < 0) - 5 Pixel Vertical Shift

Database	Samples	Mean	Median	95% CI	S-Value	P-Value
A1originalH	28900	-0.287	-0.069	$(-\pi, -0.066)$	11580	2.2e-16
Chall1H	40000	-0.556	-0.251	$(-\pi, -0.244)$	11481	2.2e-16
Chall2H	25600	-0.517	-0.316	$(-\pi, -0.305)$	7991	2.2e-16
Kitchen1H	11664	-0.309	-0.084	$(-\pi, -0.074)$	4859	2.2e-16
Moeller1H	58564	-0.285	-0.052	$(-\pi, -0.049)$	26075	2.2e-16
RobISLab	5184	-0.841	-0.659	$(-\pi, -0.621)$	1140	2.2e-16

Sign Test (With Alt. Hyp. HiSS-Warping < 0) - 15 Pixel Vertical Shift

Database	Samples	Mean	Median	95% CI	S-Value	P-Value
A1originalH	28900	-0.778	-0.528	$(-\pi, -0.513)$	6654	2.2e-16
Chall1H	40000	-0.734	-0.409	$(-\pi, -0.399)$	9888	2.2e-16
Chall2H	25600	-0.724	-0.541	$(-\pi, -0.525)$	6702	2.2e-16
Kitchen1H	11664	-0.307	-0.079	$(-\pi, -0.067)$	5016	2.2e-16
Moeller1H	58564	-0.535	-0.243	$(-\pi, -0.234)$	20712	2.2e-16
ISLab	5184	-0.927	-0.915	$(-\pi, -0.874)$	1133	2.2e-16

Sign Test (With Alt. Hyp. HiSS-Warping < 0) - 24 Pixel Vertical Shift

Database	Samples	Mean	Median	95% CI	S-Value	P-Value
A1originalH	28900	-0.885	-0.718	$(-\pi, -0.703)$	5903	2.2e-16
Chall1H	40000	-0.867	-0.638	$(-\pi, -0.625)$	8217	2.2e-16
Chall2H	25600	-0.812	-0.697	$(-\pi, -0.683)$	6057	2.2e-16
Kitchen1H	11664	-0.375	-0.133	$(-\pi, -0.120)$	4796	2.2e-16
Moeller1H	58564	-0.609	-0.386	$(-\pi, -0.376)$	18772	2.2e-16
ISLab	5184	-0.665	-0.606	$(-\pi, -0.573)$	1512	2.2e-16

Figure 20: Tables representing the results from the sign test applied to angular error data for HiSS-Warping.

5.4 Homing Success / Correlations

As well as developing an algorithm for accurate visual homing, we wish to develop a method for predicting homing success. Given two input images for homing, is there any way to use homing in scale space to predict whether or not homing will succeed without actually moving the robot? This problem applies to [x]. In order to answer this question, we first look at what kinds of data are produced by our homing method.

The first type of data we will investigate is the percentage of keypoints from the CV image which have found a match in the SS image. Intuitively, the higher percentage of keypoints matched between CV and SS, the more similar the images are, and the greater number of keypoints available for the homing in scale space algorithm to work with. Due to the nature of the algorithm, we would expect this to yield more accurate results.

The second idea for predicting homing success involves analyzing the centers of expansion and contraction. Ideally we know that translation within an environment causes the centers of expansion and contraction to be separated by 180°. We can then define γ as

$$\gamma \quad = \quad ||\bar{\theta}_{pos} - \bar{\theta}_{neg}| - 180^{\circ}| \tag{23}$$

which under ideal conditions would yield $\gamma = 0$. Values of γ which stray from zero would then indicated that our calculated centers do not align opposite to each other, and we would expect inaccurate results to follow.

Measure	AE	Dist	RR	$M_{\%}$	M_{γ}	M_{σ}
AE	1.000	0.381	-0.232	-0.388	0.162	0.359
Dist	0.381	1.000	-0.248	-0.959	0.085	0.850
RR	-0.232	-0.248	1.000	0.242	-0.144	-0.207
$M_{\%}$	-0.388	-0.959	0.242	1.000	-0.142	-0.845
M_{γ}	0.162	0.085	-0.144	-0.142	1.000	0.118
M_{σ}	0.359	0.850	-0.207	-0.845	0.118	1.000

Figure 21: Data Correlations for A1OriginalH with 0 pixel vertical shift

The last measure we will use is the standard deviation of the horizontal length of the matched correspondence vectors between SS and CV. Intuitively, the longer the horizontal length of these correspondences, the greater the shift the features have undergone in the image, and we would expect less accurate results. Given our set of correspondences $M = \{m_1, m_2, ..., m_n\}$ we calculate the standard deviation M_{σ} of all $m \in M_{std} = |m_{k_{cv_x}} - m_{k_{ss_x}}|$ for all $k \in [1, n]$.

$$M_{\sigma} = \sqrt{\frac{1}{N}\left(\sum_{k=1}^{n} |m_i - \bar{m}_i|\right)^2} \tag{24}$$

Since our data is not normally distributed, we will be using the Spearman method (also known as Spearman's ρ) [34] to calculate our correlation coefficients. The Spearman method is a non-parametric measure of rank correlation between data sets. It works in much the same way as the standard Pearson method of determining correlation, with the added step of converting the raw scores into a ranking system based on the total data set. The final output is the correlation between the ranks of the data sets, which has been shown to be more robust under non normal data,

as well as for showing non linear correlations [35].

The table in figure 21 shows sample correlation data from the A1OriginalH database trial under no vertical shift. Each trial performed on the other databases yielded similar results. We can see that there are several high correlation coefficients present in the matrix, which are also high in each of the other database trials. This highest is a negative correlation is between $M_{\%}$ and the true distance to the goal, which tells that as we get closer to the goal location, the percentage of keypoints matched gets higher. This observation goes along with our prediction earlier. Another strong correlation is between M_{σ} and distance. As we get closer to the goal, the horizontal length of our correspondence vectors shrink.

In order to predict homing success, we would need to see high correlations to angular error or return ratio. Unfortunately, we did not see these high correlations in our data, with values only reaching 0.4 as opposed to the 0.95 we see in our distance correlation. However, due to these extremely high correlations with true measured distance to the goal, we will use the highest of these, $M_{\%}$, as a way to attempt to predict the distance in our live trials.

5.5 Distance Estimation

In order to properly return an agent to a goal, it is not only necessary that we have an accurate homing angle, but we must also have an accurate distance estimation in order to stop the agent at the goal location. If there is no notion of the distance between **cv** and **ss**, the robot will simply oscillate around the goal location with

no means to come to a complete stop. As shown in the previous section, there is a very high correlation between the true distance to the goal and the percentage of keypoints matched $M_{\%}$. In figure [x] we can see that this high level of correlation is due to a seemingly exponential relationship between $M_{\%}$ and the true distance d. Using this observation, we will attempt to find a function fitting the form $d = ae^{bM_{\%}}$ using nonlinear regression. We performed nonlinear regression using the R stats package nls() nonlinear least squares function. Each of the following images shows the results of using nonlinear regression on each database in order to find a distance estimation function. The graphs show 4 functions (one for each of the 0, 5, 15, 24 pixel vertical shifts) overlayed on a plot of $M_{\%}$ vs. distance d. Note that due to the similarity of the resulting values of a and b the lines are difficult to distinguish. The tables show the computed values of a and b for the functions $d = ae^{bM_{\%}}$, as well as the standard errors for a and b, and the residual standard error for the method.

We can see by figures 22 and 23 that the distance estimation function fits nicely to the exponential curve. The function also remains remarkably similar despite large vertical shifting within the image (represented by the different lines), making this method for distance estimation feasible for environments without level movement surfaces. One downside to this approach however is that as the true distance from the goal increases, so does the error in the function. At areas in the graph where the slope of the computed function has a larger magnitude, similar values of $M_{\%}$ can yield dramatically different distances. This would lead us to believe that this distance estimation method will be less accurate for long range homing, but become more accurate as we approach the goal.

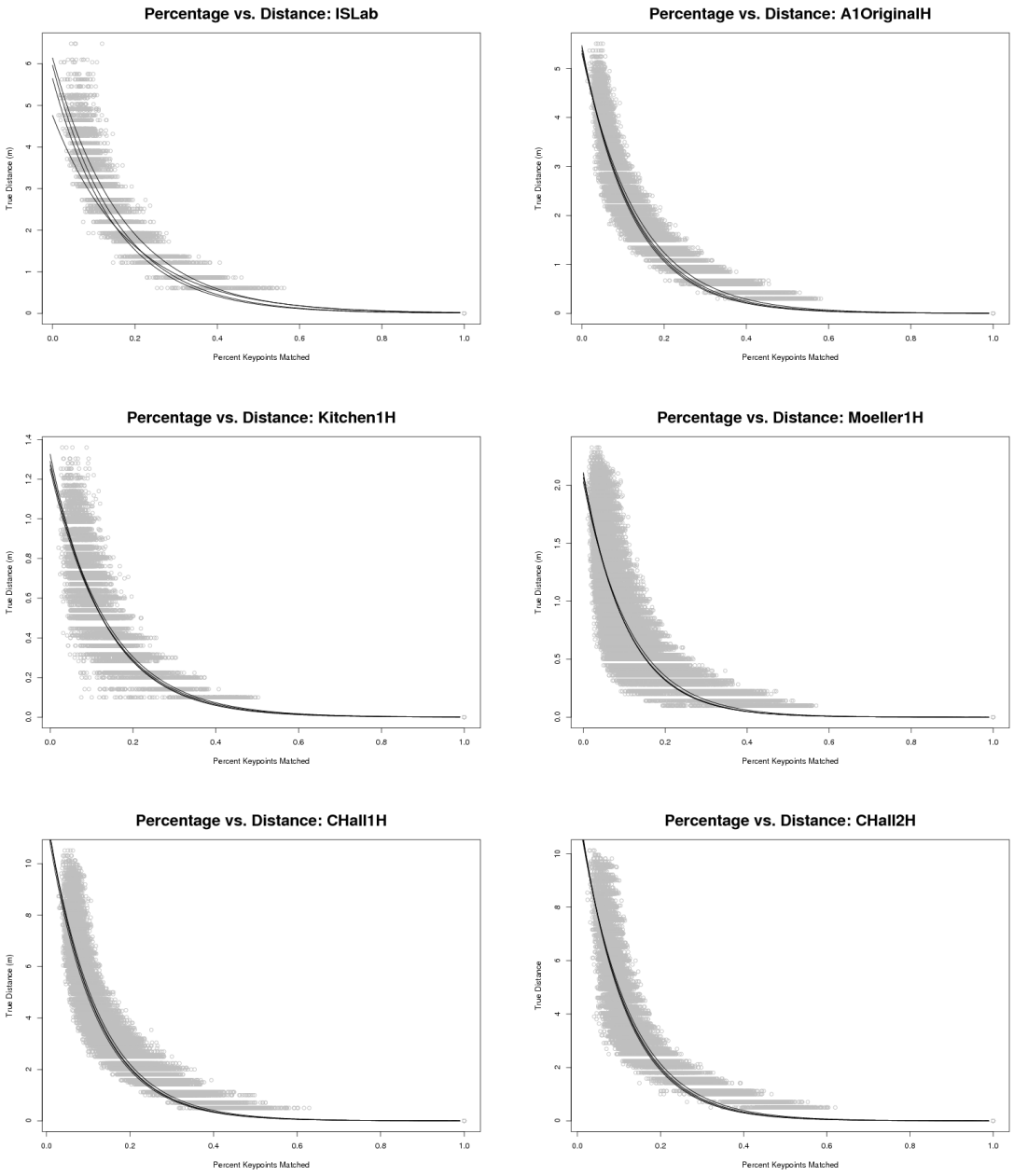

Figure 22: Percentage Matched vs. Distance graphs for each database

Database	Trial	a	b	a std. err	b std. err	RSE
Islab	0px Vert	10.06780	-5.85665	0.05436	0.04763	0.8335
	5px Vert	9.78177	-6.43592	0.06124	0.06236	0.9595
	15px Vert	9.26169	-6.53532	0.06932	0.07979	1.144
	24px Vert	7.8007	-5.4061	0.0731	0.1028	1.494
A1OriginalH	0px Vert	17.68985	-7.27702	0.03602	0.02122	1.24
	5px Vert	17.89868	-7.73030	0.03793	0.02307	1.269
	15px Vert	18.23209	-8.03045	0.04010	0.02428	1.286
	24px Vert	18.11404	-8.17131	0.04154	0.02585	1.344
CHall1H	0px Vert	23.85965	-8.45522	0.05915	0.02441	1.668
	5px Vert	23.85637	-8.75030	0.06172	0.02625	1.734
	15px Vert	23.82518	-8.82529	0.06291	0.02698	1.772
	24px Vert	23.32249	-8.90887	0.06561	0.02945	1.907
CHall2H	0px Vert	23.37360	-8.50571	0.08667	0.03625	1.88
	5px Vert	23.71199	-8.87797	0.09259	0.03905	1.941
	15px Vert	24.10059	-9.11256	0.10206	0.04246	2.037
	24px Vert	24.07061	-9.26291	0.10868	0.04574	2.144
Kitchen1H	0px Vert	12.71268	-7.15042	0.07095	0.05730	1.447
	5px Vert	12.91063	-7.58406	0.07962	0.06509	1.53
	15px Vert	13.26301	-7.77610	0.08449	0.06660	1.538
	24px Vert	12.50825	-7.31220	0.09264	0.07631	1.76
Moeller1H	0px Vert	20.28980	-8.72208	0.05359	0.03502	2.685
	5px Vert	20.66887	-9.24524	0.05959	0.03914	2.787
	15px Vert	21.09868	-9.46355	0.06302	0.04028	2.808
	24px Vert	21.01630	-9.41256	0.06539	0.04160	2.886

Figure 23: Table of results for functions plotted in figure 22. a and b correspond to the values output by performing non linear regression on function $d = ae^{bM_{\%}}$. Standard errors for a and b, as well as the residual standard error (RSE) are also included.

Another issue of note is the fact that this function varies with image dimensions. Homing within an environment using images with a height of 50 pixels will yield a different distance estimation function than an image with a height of 100 pixels. Experimentally, we have found that as resolution increases, more keypoints are found, and a higher value for $M_{\%}$ results.

5.6 ISLab Trials

To test this algorithm on our live robot, we used the same environment as used in the ISLab database. Five different goal locations were chosen, with 5 starting locations for each goal location spaced evenly throughout the environment. The robot takes an image at its current location, compares it to the goal image, computes the estimated distance and homing angle, and moves that amount in that direction. This process repeats until the robot believes it is within 30cm of the goal (success) or for a maximum of 12 iterations (failure). The distance estimation function used for the homing in scale space method was found by using the ISLab image database as a training set. A real-time distance estimation function calculator is discussed in the future work section.

It was our original intention to compare homing in scale space to the warping method by using both visual homing methods to conduct in-lab trials. Upon attempting visual homing in the ISLab using the warping method, it was found to be too inaccurate to carry out the trials. Of several dozen initial tests, the robot would almost inevitably veer off of the allotted limits for navigation. We suspect this is

due to the nature of the images captured by the robot. Due to the robot wheels being imperfectly shaped, the height of the camera affixed to the top of the robot varies between 1-2cm throughout the course of a full revolution of the robot's wheels. Since the warping method relies heavily on the stability of the horizon within an image, we believe that this variance caused enough shift of the image horizon to cause the warping method to perform poorly. Due to this, results for live trials using the warping method were not included.

We will define two types of success with respect to visual homing for our live robot trials. Type A success means the robot came to stop within both an estimated distance of 30cm and an actual distance of 30cm. Type B success means that at some point the robot came within a true distance of 30cm of the goal, however did not stop due to error in its distance estimation. If the robot stopped within 30cm of the goal at any intermediary step during a trial, but estimated it was not within the threshold, we will record it as having been an undetected arrival (UA). Therefore, type B success is equivalent to any trial which recorded an undetected arrival without achieving type A success. Figures 24 through 28 show results for each of the robot trial paths, along with a table of the associated estimated distance, actual distance, and distance estimate error for the final stage of the homing trial.

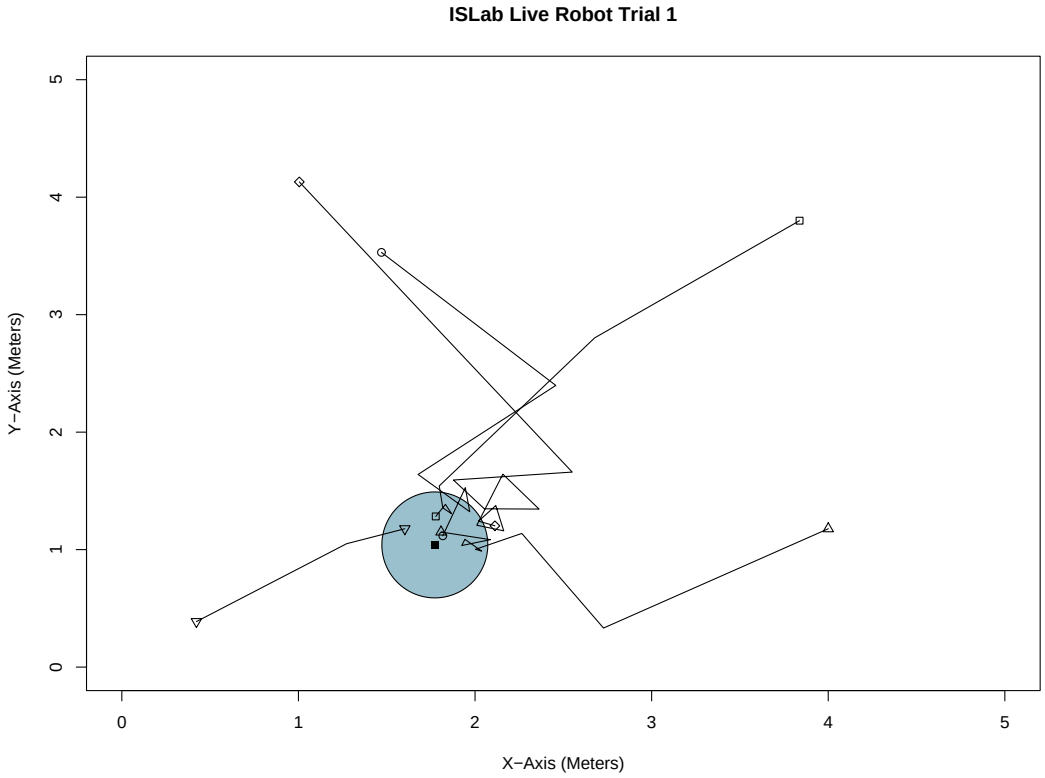

Trial		Est Dist	Act Dist	Error	Success	UA	Steps
1	○	0.25	0.09	0.16	A	NO	5
	□	0.3	0.24	0.06	A	YES	6
	◇	0.43	0.38	0.05	B	YES	12
	△	0.26	0.12	0.14	A	YES	7
	▽	0.28	0.22	0.06	A	NO	2

Figure 24: ISLab Live Homing Trial 1

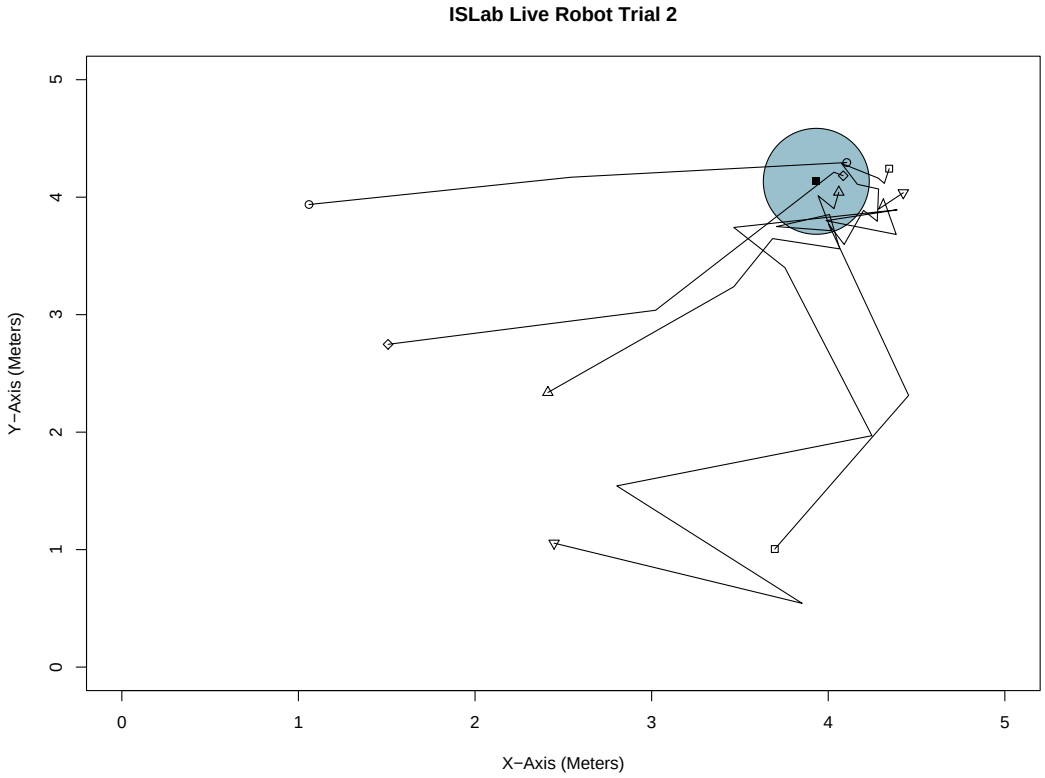

Trial		Est Dist	Act Dist	Error	Success	UA	Steps
2	○	0.29	0.24	0.06	A	NO	2
	□	0.57	0.43	0.15	A	YES	12
	◇	0.23	0.16	0.07	A	YES	3
	△	0.29	0.16	0.13	A	YES	9
	▽	0.62	0.50	0.12	NO	NO	12

Figure 25: ISLab Live Homing Trial 2

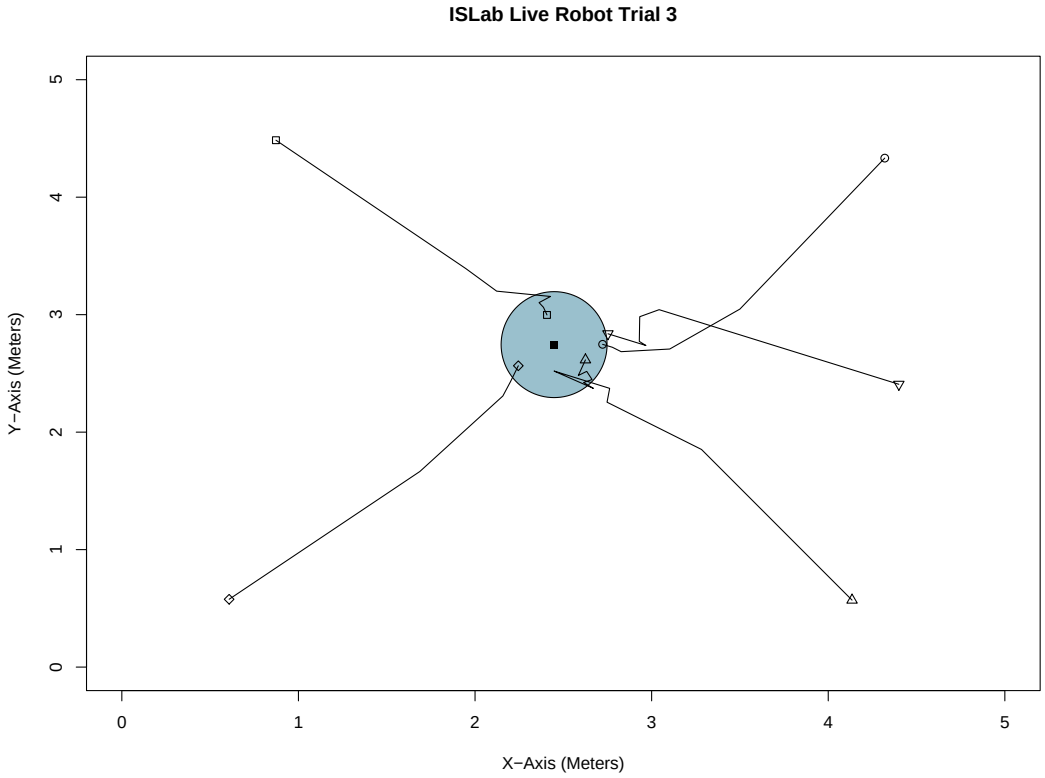

Trial		Est Dist	Act Dist	Error	Success	UA	Steps
3	○	0.29	0.27	0.02	A	NO	5
	□	0.28	0.26	0.02	A	NO	6
	◇	0.27	0.27	0.00	A	NO	4
	△	0.29	0.22	0.07	A	YES	10
	▽	0.29	0.32	0.03	A	NO	5

Figure 26: ISLab Live Homing Trial 3

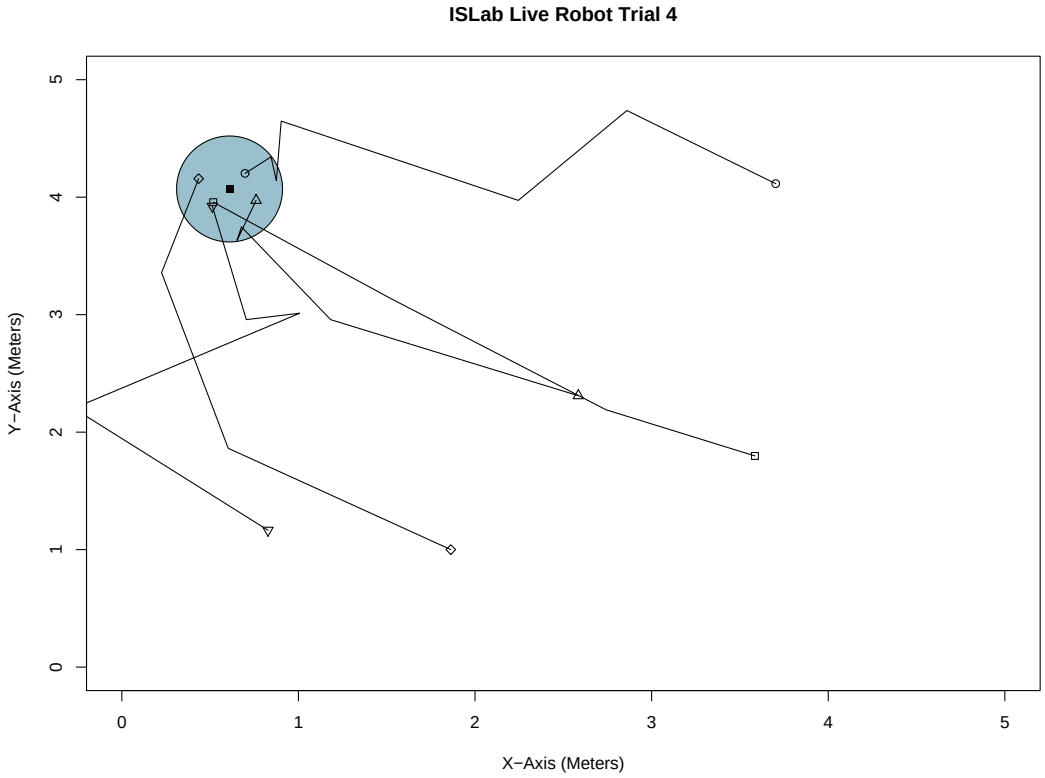

Trial		Est Dist	Act Dist	Error	Success	UA	Steps
4	○	0.27	0.16	0.12	A	YES	6
	□	0.27	0.15	0.12	A	NO	3
	◇	0.24	0.20	0.05	A	NO	3
	△	0.25	0.18	0.07	A	NO	4
	▽	0.27	0.18	0.09	A	NO	4

Figure 27: ISLab Live Homing Trial 4

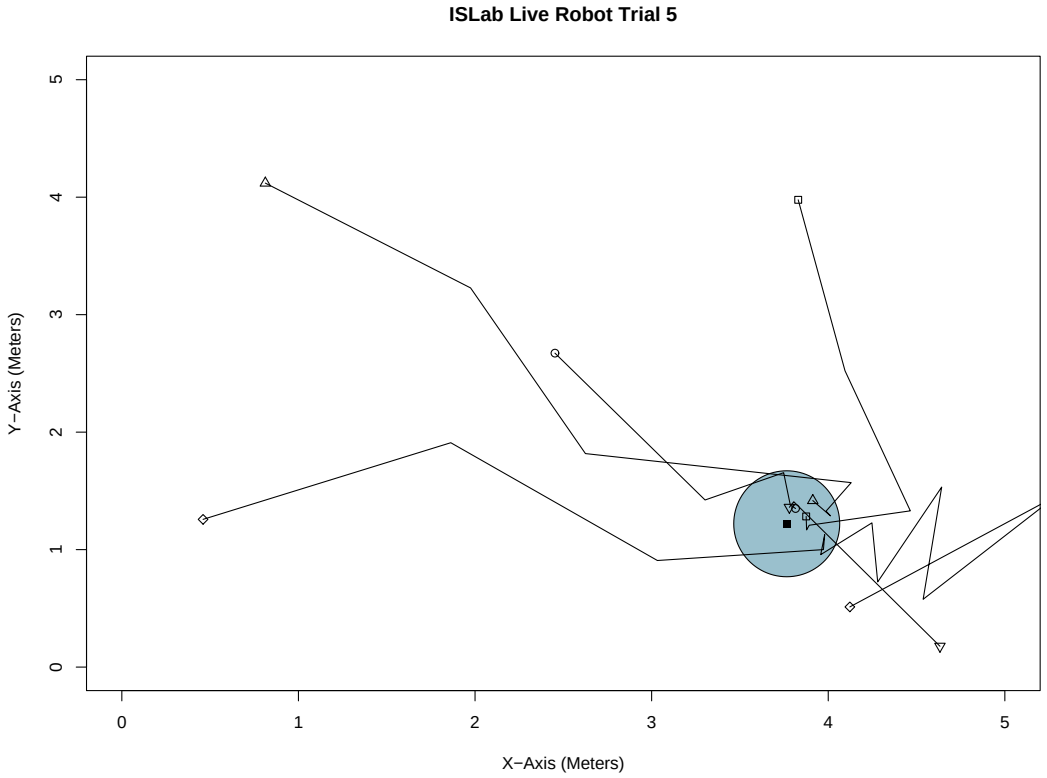

Trial		Est Dist	Act Dist	Error	Success	UA	Steps
5	○	0.28	0.14	0.14	A	YES	4
	□	0.26	0.13	0.13	A	YES	5
	◊	N/A	0.79	N/A	B	YES	12
	△	0.25	0.25	0.00	A	YES	6
	▽	0.29	0.14	0.15	A	YES	2

Figure 28: ISLab Live Homing Trial 5

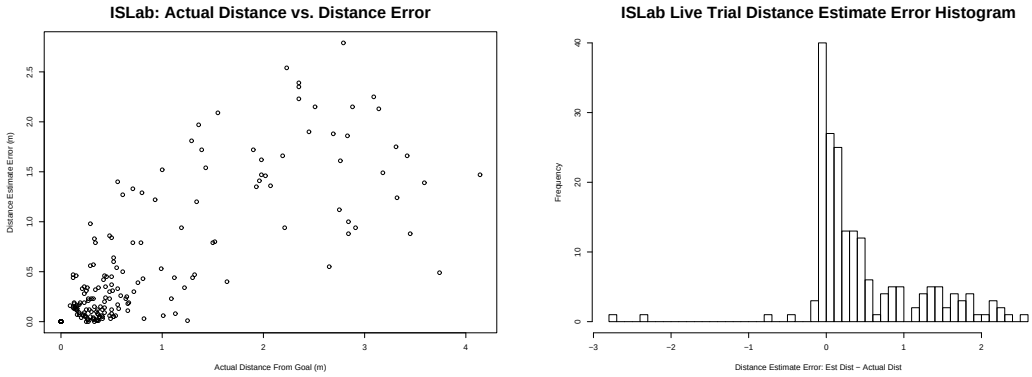

Figure 29: Graph (left) of actual distance from goal d_a vs. distance error $d_{err} = |d_e - d_a|$, along with the associated distance estimate error histogram (right).

For the 25 homing trials conducted, 21 of them resulted in type A success, 3 resulted in type B success, and only one resulted in failure. 13 of the trials resulted in the recording of an undetected arrival, which means that the method is method is actually getting closer to the goal than its distance estimation function would lead us to believe.

We can see by this graph in figure 29 that as d_a increases, so does d_{err}. Using the Spearman method of correlation between these two values yields a correlation coefficient of 0.784, which strongly reinforces this relationship. The second graph is a histogram of $d_e - d_a$, showing a possible reason for the high number of UAs in the live trials. The distance estimation function nearly always returns a value which is higher than that of the actual distance to the goal, resulting in the robot thinking it is further away from where it is, with a mean of 0.462m and a median of 0.195cm. A possible reason for this is the fact that the distance estimation function

was computed from the ISLab database, in which images were spaced 61cm apart. This larger spacing between images may yield higher error values for the estimate when actual distance is less than that of the database image spacing.

6 Conclusion

Our tests have shown that homing in scale space has outperformed the one dimensional warping method for all six image databases. Homing in scale space yielded a dramatically lower angular error, as well as a higher return ratio than the warping method, especially in images that had undergone vertical shifting. By randomly rotating our images we have shown that our method achieves complete rotation invariance for visual homing.

Our live robot trials in the Intelligent Systems laboratory have showed us that not only does the method work well for image databases, but the method is capable of achieving high rates of homing success on a live robot, with type A success rate of 84%. If we combine this with our type B successes, we see that homing in scale space was able to bring the robot to within 30cm of the goal in 24 of the 25 of the trials. All of this was achieved in an environment under which the warping method failed to produce results accurate enough to be meaningfully recorded.

6.1 Afterthought

Several ideas relating to homing in scale space were thought of throughout the course of this research, but due to time constraints were not able to be fully explored.

The first of these ideas was the scale difference threshold. Recall the value of $\beta = \sigma_{ss} - \sigma_{cv}$ which determined whether or not a keypoint was classified as belonging to the region of contraction or expansion. In cases of images which were taken at locations which were very close together, we would see many very small values for β.

If we combine these values which are very close to zero with factors such as noise or improper camera focus, we see that these keypoints may be misclassified. The scale difference threshold would be some value T_β for which keypoints which had values of $|\beta| < T_\beta$ would be discarded. Initial exploration into this idea yielded better results for some databases, while yielding worse results for others. A possible reason for this could be due to the spacing between images in a given database. Possible future work may include scaling T_β based on image spacing to produce overall better homing results.

Distance estimation was another area where improvements could be made. The distance estimation formula which was used in our live robot trials was computing using nonlinear regression based on data from data collected from the ISLab database. We propose that a distance estimation function for a particular environment could be calculated by odometry data from a live robot, eliminating the need for an existing database. To do this, the robot would first need to acquire an image of a goal location within the environment. As the robot then moved around to various locations, true distance from odometry could be compared to the value of $M_\%$ used to calculate the distance estimation function. If some incremental version of nonlinear regression was then used, the estimation function could not only be calculated live, but could grow increasingly accurate as the robot continued to navigate. This continuous movement within an environment would also cover a much wider range of distances than the discretely spaced database model, possibly yielding more accurate results.

A new database of images is needed for testing visual homing under arbitrary

3D transformations. Such a database would need to be captured not only along a grid of different locations, but at varying elevations and 3D orientations as well. Our attempts at simulating vertical shifting in images is obviously flawed due to the missing region of the image, but also due to the lack of change in 3D perspective which would be present in a real elevation shift. If this database was captured in outdoor as well as indoor environments, it would allow for a much better overall comparison of visual homing algorithms.

The ultimate end goal of homing in scale space will be to apply the method to unmanned aerial vehicles (UAVs). The lack of constraints on the presence of an image horizon should allow this method to be applied to situations where more arbitrary transformations are performed. Since aerial vehicles can navigate in six degrees of freedom, our new homing vector would contain not only the angle of rotation θ_{homing} but an angle of elevation φ_{homing} as well. θ_{homing} would still be calculated by the angular mean of $f_{\theta x}$, while φ_{homing} would be calculated by the angular mean of $f_{\theta y}$ for a given set of keypoints. With these angles, along with an estimated distance from the goal, visual homing in UAVs would be possible.

References

[1] B. Cartwright and T. Collett, "Landmark learning in bees," *Journal of Comparative Physiology A*, vol. 151, pp. 521–543, 1983.

[2] M. Franz, B. Schölkopf, P. Georg, H. Mallot, and H. Bülthoff, "Learning view graphs for robot navigation," in *Proceedings of the First International Conference on Autonomous Agents (Agents'97)*, W. L. Johnson and B. Hayes-Roth, Eds. ACM Press, 1997, pp. 138–147.

[3] R. Möller and A. Vardy, "Local visual homing by matched-filter descent in image distances," *Biological Cybernetics*, vol. 95, pp. 413–430, 2006.

[4] D. Lowe, "Distinctive image features from scale-invariant keypoints," *International Journal of Computer Vision*, vol. 60, no. 2, pp. 91–110, 2004.

[5] T. Collett and M. Collett, "Memory use in insect visual navigation," *Nature Reviews Neuroscience*, vol. 3, pp. 542–552, 2002.

[6] A. Argyros, C. Bekris, S. Orphanoudakis, and L. Kavraki, "Robot homing by exploiting panoramic vision," *Journal of Autonomous Robots*, vol. 19, no. 1, pp. 7–25, 2005.

[7] A. Vardy, "Long-range visual homing," in *Proceedings of the IEEE International Conference on Robotics and Biomimetics*. IEEE Xplore, 2006.

[8] M. Franz, B. Schölkopf, H. Mallot, and H. Bülthoff, "Learning view graphs for robot navigation," *Autonomous Robots*, vol. 5, pp. 111–125, 1998.

[9] W. Hübner and H. Mallot, "Metric embedding of view-graphs: A vision and odometry-based approach to cognitive mapping," *Autonomous Robots*, vol. 23, p. 183196, 2007.

[10] J. Zeil, M. Hofmann, and J. Chahl, "Catchment areas of panoramic snapshots in outdoor scenes," *Journal of the Optical Society of America A*, vol. 20, no. 3, pp. 450–469, 2003.

[11] A. Vardy and R. Möller, "Biologically plausible visual homing methods based on optical flow techniques," *Connection Science*, vol. 17, no. 1/2, pp. 47–90, 2005.

[12] J. S. Pons, W. Hübner, J. Dahmen, and H. Mallot, "Vision-based robot homing in dynamic environments," in *13th IASTED International Conference on Robotics and Applications*, K. Schilling, Ed., 2007, pp. 293–298.

[13] A. Rizzi, D. Duina, S. Inelli, and R. Cassinis, "Unsupervised matching of visual landmarks for robotic homing using Fourier-Mellin transform," in *Intelligent Autonomous Systems 6*, 2000, pp. 455–462.

[14] A. Vardy and F. Opacher, "Low-level visual homing," *Advances in Artificial Life - Proceedings of the 7th European Conference on Artificial Life*, pp. 875–884, 2003.

[15] J. Hong, X. Tan, B. Pinette, R. Weiss, and E. Riseman, "Image-based homing," in *Proceedings of the 1991 IEEE International Conference on Robotics and Automation, Sacremento, CA*, 1991, pp. 620–625.

[16] S. V. K. Weber and M. Srinivassan, "Insect-inspired robotic homing," *Adaptive Behaviour*, pp. 65–97, 1999.

[17] D. Lambrinos, R. Möller, T. Labhart, R. Pfeifer, and R. Wehner, "A mobile robot employing insect strategies for navigation," *Robotics and Autonomous Systems, Special Issue: Biomimetic Robots*, vol. 30, pp. 39–64, 2000.

[18] A. Briggs, Y. Li, D. Scharstein, and M. Wilder, "Robot navigation using 1d panoramic images," in *International Conference on Robotics and Automation*, 2006, pp. 2679–2685.

[19] T. Goedemé, M. Nuttin, T. Tuytelaars, and L. Van Gool, "Omnidirectional vision based topological navigation," *International Journal of Computer Vision*, vol. 74, no. 3, pp. 219–236, 2007.

[20] D. L. S. Se and J. Little, "Mobile robot localization and mapping with uncertainty using scale-invariant visual landmarks," *Int. J. Robot. Res.*, vol. 21, pp. 39–64, 2001.

[21] A. Vardy and R. Möller, "Panoramic image database," 2008. [Online]. Available: http://www.ti.uni-bielefeld.de/html/research/avardy/index.html

[22] R. Möller, A. Vardy, S. Kreft, and S. Ruwisch, "Visual homing in environments with anisotropic landmark distribution," *Autonomous Robots*, vol. 23, pp. 231–245, 2007.

[23] "The r project for statistical computing," 2008. [Online]. Available: http://www.r-project.org/

[24] M. Franz, B. Schölkopf, H. Mallot, and H. Bülthoff, "Where did I take that snapshot? Scene-based homing by image matching," *Biological Cybernetics*, vol. 79, pp. 191–202, 1998.

[25] MobileRobots, "The high-performance all-terrain robot (p3-at)," 2008. [Online]. Available: http://www.activrobots.com/ROBOTS/p2at.html

[26] ——, "Advanced robotics interface for applications (aria) robotic sensing and control libraries," 2008. [Online]. Available: http://www.activrobots.com/SOFTWARE/aria.html

[27] ——, "Mobilesim, the mobilerobots simulator," 2008. [Online]. Available: http://robots.mobilerobots.com/MobileSim/README.html

[28] P. Royston, "An extension of shapiro and wilk's w test for normality to large samples," in *Applied Statistics*, 1982, pp. 115–124.

[29] ——, "Algorithm as 181: The w test for normality," in *Applied Statistics*, 1982, pp. 176–180.

[30] ——, "A remark on algorithm as 181: The w test for normality," in *Applied Statistics*, 1995, pp. 547–551.

[31] J. Gibbons and S. Chakraborti, *Nonparametric Statistical Inference*. Marcel Dekker Inc., New York, 1992.

[32] L. Kitchens, *Basic Statistics and Data Analysis*. Duxbury, 2003.

[33] E. L. Lehmann, *Nonparametrics: Statistical Methods Based on Ranks.* Holden and Day, San Francisco, 1975.

[34] C. Spearman, "The proof and measurement of association between two things," *Amer. J. Psychol.*, vol. 15, pp. 72–101, 1904.

[35] M. Kendall, *Rank correlation methods.* Griffin, 1962.